

1                                   **A Cryptochrome 2 Mutation Yields**  
2                                   **Advanced Sleep Phase in Human**

3  
4 Arisa Hirano<sup>1</sup>, Guangsen Shi<sup>1</sup>, Christopher R. Jones<sup>2</sup>, Anna Lipzen<sup>3,4</sup>, Len A.  
5 Pennacchio<sup>3,4</sup>, Ying-Xu<sup>5</sup>, William C. Hallows<sup>1</sup>, Thomas McMahon<sup>1</sup>, Maya  
6 Yamazaki<sup>1</sup>, Louis J. Ptáček<sup>1,6\*</sup>, Ying-Hui Fu<sup>1\*</sup>

7  
8 <sup>1</sup>Department of Neurology, University of California San Francisco, San  
9 Francisco, 94143, CA

10 <sup>2</sup>Department of Neurology, University of Utah, Salt Lake City, UT

11 <sup>3</sup>Lawrence Berkeley National Laboratory, Berkeley, CA

12 <sup>4</sup>Department of Energy Joint Genome Institute, Walnut Creek, CA

13 <sup>5</sup>Center for System Biology, Soochow University, Suzhou, China

14 <sup>6</sup>Howard Hughes Medical Institute, University of California San Francisco, San  
15 Francisco, CA

16  
17 \*Correspondence: L.J.P. ([ljp@ucsf.edu](mailto:ljp@ucsf.edu)), Y-H.F. ([Ying-Hui.Fu@ucsf.edu](mailto:Ying-Hui.Fu@ucsf.edu)).  
18  
19  
20  
21  
22  
23  
24

25 **Abstract**

26 Familial Advanced Sleep Phase (FASP) is a heritable human sleep phenotype  
27 characterized by very early sleep and wake times. We identified a missense  
28 mutation in the human Cryptochrome 2 (*CRY2*) gene that co-segregates with  
29 FASP in one family. The mutation leads to replacement of an alanine residue at  
30 position 260 with a threonine (A260T). In mice, the *CRY2* mutation causes a  
31 shortened circadian period and reduced phase-shift to early-night light pulse  
32 associated with phase-advanced behavioral rhythms in the light-dark cycle. The  
33 A260T mutation is located in the phosphate loop of the flavin adenine  
34 dinucleotide (FAD) binding domain of *CRY2*. The mutation alters the  
35 conformation of *CRY2*, increasing its accessibility and affinity for FBXL3 (an E3  
36 ubiquitin ligase), thus promoting its degradation. These results demonstrate that  
37 *CRY2* stability controlled by FBXL3 plays a key role in the regulation of human  
38 sleep wake behavior.

39

40

41

42

43

44

45

46 **Introduction**

47 Sleep is vital for all animals. Sleep-wake timing is regulated by the internal  
48 biological clock driving physiological rhythms with a period of approximately 24  
49 hours (Takahashi, 1995). The circadian clock is composed of interlocked  
50 transcriptional and translational negative feedback loops (Lowrey and Takahashi,  
51 2004; Reppert and Weaver, 2001). In mammals, a CLOCK-BMAL1 heterodimer  
52 binds to E-boxes and activates gene expression of the *Period (Per)* and  
53 *Cryptochrome (Cry)* genes. Translated PERs and CRYs proteins form a complex  
54 that enters the nucleus to inhibit their own transcription through direct interaction  
55 with CLOCK-BMAL1 heterodimers. PER and CRY proteins accumulating in the  
56 nucleus are then degraded over time. As protein levels fall (depending on rate of  
57 degradation), the transcription-translation feedback loop begins anew.

58 *CRY2* is a principal component in mammalian circadian clocks (Shearman  
59 et al., 2000; van der Horst et al., 1999; Vitaterna et al., 1999). While *Drosophila*  
60 and plant CRY proteins act as photoreceptors contributing to photoentrainment  
61 of the circadian clock and other biological processes by binding to flavin adenine  
62 dinucleotide (FAD) (Partch and Sancar, 2005), mammalian CRY2 has  
63 light-independent transcriptional repressor activity and strongly inhibits  
64 E-box-regulated gene expression (Griffin et al., 1999; Kume et al., 1999;  
65 Shearman et al., 2000). The protein stability of CRY2 is fine-tuned by  
66 post-translational modification including phosphorylation and ubiquitylation. In  
67 addition, various enzyme modifications play a role in CRY2 regulation (Reischl

68 and Kramer, 2011; Stojkovic et al., 2014). Among them, FBXL3 is an F-box type  
69 E3 ubiquitin ligase which promotes CRY1 and CRY2 ubiquitylation thus leading  
70 to proteasome-mediated degradation (Busino et al., 2007). Mutations in mouse  
71 *Fbxl3* or knockout of the *Fbxl3* gene dramatically lengthens the period of mouse  
72 behavioral rhythms in constant darkness (Godinho et al., 2007; Hirano et al.,  
73 2013; Shi et al., 2013; Siepka et al., 2007), indicating that the protein stability of  
74 CRY1 and CRY2 is a critical determinant of circadian period in mice. However,  
75 direct evidence supporting the significance of *CRY2* and the post-translational  
76 regulation of *CRY2* protein in the human circadian clock regulating the  
77 sleep-wake cycle has been lacking.

78       Familial Advanced Sleep Phase (FASP) is a heritable sleep phenotype  
79 characterized by stable early sleep and wake times (Jones et al., 1999; Reid and  
80 Burgess, 2005; Reid et al., 2001). The FASP phenotype can segregate as a  
81 highly penetrant, autosomal dominant trait in human kindreds. Previously, we  
82 have identified mutations in clock genes, including *Period2*, *Period3*, *casein*  
83 *kinase 1 $\delta$* , and *Dec2* causing circadian and sleep homeostasis phenotypes in  
84 humans (He et al., 2009; Toh et al., 2001; Xu et al., 2005; Zhang et al., 2016). A  
85 mutation at the phosphorylation priming site of PER2 attenuates sequential  
86 phosphorylation and consequently destabilizes PER2 proteins. The mouse  
87 model expressing mutant PER2 exhibits a shortened circadian period  
88 accompanied with large phase-advance in sleep-wake rhythms (Xu et al., 2007).  
89 This sequential phosphorylation region of PER2 was later found to be modulated

90 by another post-translational regulation, O-GlcNAcylation, demonstrating an  
91 interplay and competition between phosphorylation and O-GlcNAcylation of  
92 serine residues in this region (Kaasik et al., 2013). These studies highlighted the  
93 important role of post-translational regulation of clock proteins *in vivo* in humans  
94 and also revealed mechanistic insight into the regulation of PER2. Thus, human  
95 genetic studies have provided valuable and unique opportunities to elucidate  
96 novel molecular mechanisms of circadian/sleep regulation.

97 Here we report the identification of a novel variant in the human hCRY2  
98 gene that leads to FASP. Generation of a mouse model carrying the mutation  
99 revealed that the mutation causes a FASP-like phenotype in mice with altered  
100 circadian period and photic entrainment. We found that the mutation in the CRY2  
101 FAD-binding-domain enhances its affinity for FBXL3, thus destabilizing CRY2 via  
102 increased ubiquitylation and targeting for degradation by the proteasome. We  
103 conclude that regulation of CRY2 stability by a proper balance of FAD and  
104 FBXL3 is essential for the sleep-wake cycle in humans.

105

## 106 **Results**

### 107 **Identification of a novel mutation in the hCRY2 gene associated with FASP**

108 Through candidate gene screening in FASP families, we identified a missense  
109 mutation in the human *CRY2* gene, which causes an amino acid conversion  
110 from Ala→Thr at position 260 (A260T) (Figure 1A). No other novel mutations  
111 were found in ~25 candidate circadian genes that were sequenced. The A260T

112 mutation is associated with the circadian phenotype in this FASP family (Figure  
113 1A) (Jones et al., 1999; Toh et al., 2001; Xu et al., 2005; Zhang et al., 2016). The  
114 fraternal twin sisters inherited the mutation from their mother and both reported a  
115 strong morning preference (Horne-Ostberg scores of 84 and 72) (Figure  
116 1-source data 1). The proband also had a very early melatonin onset (4:41 P.M.),  
117 while the averaged melatonin onset of normative samples is 8:50 P.M. (Burgess  
118 and Fogg, 2008). Her melatonin onset time is 3.35 standard deviations earlier  
119 than expected and among the earliest 0.05% of normative samples (Burgess  
120 and Fogg, 2008). Ala260 is located in the FAD binding domain of CRY2 and it is  
121 highly conserved in CRY1 and CRY2 proteins of various species (Figure 1B).

122

### 123 **FASP in mouse model carrying A260T mutation**

124 To test whether the A260T mutation causes FASP and has a dominant effect on  
125 the circadian sleep-wake cycle, we generated wild-type hCRY2 (*hCRY2-WT*)  
126 and mutant hCRY2 (*hCRY2-A260T*) human BAC transgenic (Tg) mice (Figure  
127 2-supplement 1A). Transgenic mice were subjected to locomotor behavioral  
128 analysis using a video camera tracking system. Under conditions of 12-hr light  
129 and 12-hr dark (LD 12:12), both *hCRY2-WT* and *hCRY2-A260T* mice entrained  
130 stably to the LD cycle (Figure 2A). However, the peak time of resting behavior,  
131 as determined by quadratic-function fitting, was significantly advanced in  
132 *hCRY2-A260T* mutant mice (Figure 2B). The activity offset and onset times were  
133 also advanced in *hCRY2-A260T* mutant mice vs. *hCRY2-WT* mice (Figure 2C

134 and Figure 2-supplement 1B). Similarly, hCRY2-A260T mutant mice on a *Cry2*  
135 null background demonstrated advanced activity onset and offset, especially  
136 around the LD transition (ZT12-13) (Figure 2-supplement 1C). These results  
137 demonstrate that hCRY2-A260T mice recapitulate the advanced sleep phase  
138 seen in the human FASP subjects harboring the *CRY2* mutation.

139

#### 140 **Shortened period and reduced phase-shift in hCRY2-A260T mice**

141 We next analyzed voluntary wheel-running activity to evaluate phase-shift and  
142 free-running period of the circadian clock for the Tg mouse models. Similar to  
143 locomotor activity measured by video tracking (Figure 2A), wheel-running  
144 activity offset times were advanced in hCRY2-A260T vs. hCRY2-WT in LD on  
145 both mCry2 WT and null backgrounds (Figure 2D; Figure2-supplements 2),  
146 while there are no significant differences in activity onset time and acrophase.  
147 Interestingly, hCRY2-A260T showed reduced phase-delay when mice were  
148 subjected to a 30-min light pulse at ZT14 (Figure 2D, E), whereas  
149 phase-advance was normal in response to a light pulse at ZT22 (Figure  
150 2-supplement 3). Thus, mutant mice have reduced sensitivity to entrainment by  
151 light at early night compared to control mice. The mice were subsequently  
152 released into constant darkness (DD) to determine circadian period. The  
153 free-running period of hCRY2-A260T (23.52±0.04 hr) was significantly shorter  
154 than that of hCRY2-WT (23.70±0.03 hr) and WT mice (23.74±0.02 hr) (Figure  
155 2F). The period shortening phenotype was further enhanced by crossing Tg

156 mice onto the mCry2 null background (Figure 2-supplement 4A). The shorter  
157 circadian period and reduced phase-delay were also observed in another mutant  
158 line (23.51±0.06 hr) with a higher mutant transgene copy number (Figure  
159 2-supplement 1A, 4B), thus excluding the possibility that the phenotype was due  
160 to positional effects of the transgene insertion site in the genome. Of note, there  
161 is no significant difference in the periods and phase-shifting of hCRY2-WT  
162 transgenic vs. transgene negative mice (Figure 2E, F), indicating that the  
163 shortening of circadian period and abnormal phase-delay are not simply due to  
164 overexpression of hCRY2. Taken together, these data demonstrate that the  
165 phase-advances in mice and humans results from the CRY2 mutation. Data from  
166 the transgenic mice suggests that the phase advance may be due to a  
167 combination of shortened period and altered sensitivity to photic entrainment.

168

#### 169 **Shortened circadian period in peripheral clocks of hCRY2-A260T**

170 The effect of the mutation on the circadian period and phase angle in the  
171 peripheral clock was examined by crossing BAC transgenic mice with mPer2<sup>LUC</sup>  
172 knock-in mice (Yoo et al., 2004). Consistent with the behavioral rhythms,  
173 shortened clock period was observed in PER2::LUC bioluminescence rhythms  
174 of liver and lung cultures from hCRY2-A260T vs. WT mice (Figure 3A, B). The  
175 peak and trough time of the bioluminescence rhythms were advanced in both  
176 tissues of hCRY2-A260T mice, suggesting that phase of the peripheral clock is  
177 also advanced by the mutation *in vivo* (Figure 3C). Circadian period shortening

178 by the A260T mutation was also found using mouse embryonic fibroblasts  
179 (MEFs) derived from mice with a mutant vs. WT transgene on both WT and  
180 mCry2 knockout backgrounds (Figure 3D, E). In addition, NIH3T3 cells stably  
181 expressing CRY2-A260T also displayed a shorter circadian period than  
182 CRY2-WT expressing cells (Figure 3F), emphasizing the dominant effect of  
183 CRY2-A260T on the circadian period. Our results indicate that CRY2-A260T  
184 shortens the circadian period in both central and peripheral clocks, consistent  
185 with current understanding that core clock genes such as *Cry2* influence  
186 physiologies in multiple mammalian organ systems.

187

#### 188 **Destabilization of CRY2 protein by the A260T mutation**

189 The CRY2 Ala260 residue resides in the “phosphate loop” responsible for  
190 binding to the phosphate of FAD (Hitomi et al., 2009) (Figure 1B). Mutations at  
191 amino acid residues critical for FAD binding affect CRY2 repressor activity of  
192 E-box-mediated transcriptional activation (Czarna et al., 2013; Hitomi et al.,  
193 2009; Sanada et al., 2004). Furthermore, Ser265 of mouse CRY2 (homologous  
194 residue of Ser266 in human CRY2) is a phosphorylation site, and the S265D  
195 mutation, mimicking a phosphorylated serine 265, reduces CRY2 repressor  
196 activity (Sanada et al., 2004). Using a Luciferase assay, we found that the A260T  
197 mutation weakened CRY2 repressor activity on *Per1* E-box-mediated  
198 transcriptional activation by CLOCK-BMAL1 (Figure 4A). However, the nuclear  
199 CRY2 protein levels in culture cells were decreased by the mutation (Figure 4B),

200 which could potentially account for the reduction of CRY2 repressor activity  
201 (Figure 4A). We then examined the degradation of CRY2 proteins by  
202 cycloheximide (CHX) chase experiments. Consistent with the cellular distribution  
203 of CRY2 (Figure 4B), CRY2-A260T was less stable than CRY2-WT in HEK293  
204 cells, especially in the nucleus (Figure 4C). Destabilization of CRY2 by the  
205 mutation was further verified in a CRY2-LUC based bioluminescence  
206 degradation assay, where the protein decay rate can be determined by recording  
207 CRY2-LUC bioluminescence in culture (Hirano et al., 2013; Hirota et al., 2012)  
208 (Figure 4-supplement 1A). Although Ala260 does not directly bind to FAD (Hitomi  
209 et al., 2009), amino acid conversion from the hydrophobic and small amino acid,  
210 alanine, to threonine could alter the conformation of the phosphate loop. This  
211 idea is supported by an observation that a mutation from alanine to aspartic acid  
212 (A260D) caused a more severe effect on CRY2 repressor activity and protein  
213 stability than the A260T mutation (Figure 4-supplement 1A, B). We found that  
214 human CRY1 harboring the corresponding mutation at position 241 is less stable  
215 than CRY1-WT, suggesting a common regulatory mechanism for CRY1 and  
216 CRY2 by FAD binding (Figure 4-supplement 1C). These results indicate that the  
217 conformation of the phosphate loop may play critical roles in regulating CRY2  
218 stability and repressor activity.

219

#### 220 **A260T mutation affects FBXL3-CRY2 interaction**

221 FBXL3 primarily localizes in the nucleus and promotes proteasomal degradation

222 of CRY2, consequently having a strong impact on the circadian period of mice  
223 (Busino et al., 2007; Godinho et al., 2007; Siepka et al., 2007; Stojkovic et al.,  
224 2014). A previous structural study demonstrated that C-terminal region of FBXL3  
225 interacts with CRY2 through the FAD binding pocket and mutations in the FAD  
226 binding domain alter CRY2-FBXL3 interaction (Xing et al., 2013). We therefore  
227 speculated that the A260T mutation affects the FBXL3-CRY2 interaction, thus  
228 altering CRY2 protein stability. We first examined WT and mutant CRY2 stability  
229 in the absence of FBXL3. As anticipated, h*FBXL3* knockdown in HEK293 cells  
230 increased the stability of both CRY2-WT and CRY2-A260T. Interestingly, the  
231 destabilizing effect of the A260T mutation was abrogated by h*FBXL3* knockdown  
232 (Figure 5A), suggesting the effect of the mutation requires FBXL3.

233 FAD stabilizes CRY2 by structurally interfering with the interaction  
234 between FBXL3 and CRY2 (Xing et al., 2013). We found that treatment of  
235 HEK293 cells with FAD increased CRY2-WT protein levels much more than  
236 CRY2-A260T (Figure 5B), suggesting that stabilization of CRY2 by FAD was  
237 reduced by the mutation. This result supports the hypothesis that the A260T  
238 mutation alters the FBXL3-CRY2 interaction. We thus carried out a competitive  
239 assay by adding FAD to complexed CRY2-FBXL3 to examine the effect of the  
240 mutation on the release of CRY2 from purified CRY2-FBXL3 complexes *in vitro*.  
241 Free CRY2-WT protein levels increased with addition of FAD in a  
242 dose-dependent manner (Figure 5C). In contrast, mutant CRY2 was released  
243 less readily than CRY2-WT from the complexes even though both forms of

244 CRY2 were bound to FBXL3 at the same level (Figure 5C). In addition, we tested  
245 FBXL3-mediated CRY2 degradation using KL001, a small synthetic molecule  
246 known to stabilize CRY1 and CRY2 (Hirota et al., 2012) due to its structural  
247 similarity to FAD (Nangle et al., 2013). KL001 stabilizes CRY2-WT in a  
248 dose-dependent manner as was previously reported (Hirota et al., 2012).  
249 However, KL001 failed to stabilize CRY2-A260T to the same extent it did for  
250 CRY2-WT (Figure 5D, Figure 5-supplement 1A). These results indicate that the  
251 A260T mutation weakened the function of FAD and KL001 as inhibitors of  
252 FBXL3-mediated degradation of CRY2 and that CRY2-A260T is less stable than  
253 CRY-WT, likely due to strengthened interaction with FBXL3. To determine  
254 whether the A260T mutation indeed modifies the interaction of CRY2 and FBXL3,  
255 we performed co-immunoprecipitation analysis. As expected, CRY2-A260T  
256 binds more strongly to FBXL3 than CRY2-WT in HEK293 cells (Figure 5E),  
257 consequently leading to more ubiquitylation of the mutant protein (Figure 5F).  
258 The effect of the mutation on the binding affinity under *in vivo* conditions will  
259 need to be further evaluated when better human CRY2 antibodies (for  
260 immunoprecipitation) become available.

261           We next performed structural modeling of mutant CRY2 to address how  
262 the A260T mutation modulates conformation of the phosphate loop. For  
263 modeling, we used the mouse CRY2 structure as the crystal structure of mouse  
264 CRY2-FBXL3 complex is available (Xing et al., 2013) and amino acid sequence  
265 in the phosphate loop perfectly conserved (Figure 1B). The published

266 CRY2-FBXL3 structure (Xing et al., 2013) revealed that space between Ala260  
267 (corresponding to A259T in mouse) and Asp442 (mouse Asp441) in  
268 FBXL3-binding form (red) is more opened vs. the FAD-binding form (orange,  
269 Figure5-supplement 1B). The amino acid change from Ala260 to Thr increases  
270 molecular density in this space and may alter electrostatic interactions between  
271 Ala260Thr and Asp442. As a result, the mutation likely renders the CRY2-A260T  
272 more accessible to FBXL3 binding (Figure5-supplement 1C). This model is  
273 consistent with the results from CRY2-A260D mutation (Figure4-supplement 1).  
274 Taken together, we demonstrated that the A260T mutation in the FAD binding  
275 pocket endows mutant CRY2 with a higher accessibility and affinity for FBXL3,  
276 therefore leading to faster proteasomal degradation of mutant vs. wild-type  
277 CRY2.

278

### 279 **Decreased endogenous CRY2 protein levels in hCRY2-A260T mice**

280 Our *in vitro* studies demonstrate that CRY2-A260T is less stable than CRY2-WT  
281 (Figure 4). To examine the protein levels of mutant vs. wild-type CRY2 under  
282 physiological conditions, we used MEFs prepared from transgenic mice. Total  
283 protein levels of endogenous CRY2 were significantly lower in synchronized  
284 cells derived from hCRY2-A260T vs. hCRY2-WT mice at two different time  
285 points (Figure 6A), even though *Cry2* transcript levels in hCRY2-A260T mice  
286 was higher than in hCRY2-WT mice (Figure 6B). Similarly, CRY2 protein levels  
287 from liver nuclear extracts were lower in hCRY2-A260T vs. hCRY2-WT mice

288 (Figure 6C, D), while hCRY2 mRNA levels were higher in mutant mice (Figure  
289 6E). CRY1 protein levels were also decreased by the mutation in nuclear  
290 extracts from liver (Figure 6C, D), suggesting that CRY1 is destabilized in  
291 hCRY2-A260T mice. At the same time, we found that nuclear expression of  
292 PER1 and PER2 were up-regulated in liver extracts from mutant mice,  
293 particularly at ZT14 (Figure 6C, D), suggesting that the timing of nuclear  
294 accumulation of PER proteins is advanced in hCRY2-A260T mice. Although  
295 PER1 and PER2 protein levels were significantly altered, their mRNA levels  
296 were not different (Figure 6E). A similar alteration of PER1 and PER2 protein  
297 levels in the absence of noticeable changes in mRNA levels was previously  
298 reported for *Psttm* mutant mouse liver (Yoo et al., 2013). *Psttm* mice have a  
299 mutation in the *Fbxl21* gene and this mutation decreases the protein level of  
300 FBXL21, which functionally competes with FBXL3. The *Psttm* mutation resulted  
301 in CRY1 and CRY2 protein destabilization and a shorter circadian period in mice  
302 (Yoo et al., 2013), which parallels the phenotype of our hCRY2-A260T mice  
303 (Figure 2E). We found that the expression of clock genes in liver was not  
304 significantly altered by the mutation, while the effect was obvious in MEFs  
305 (Figure 6B, E, and Figure 6-supplement 1). This is congruent with a previous  
306 suggestion that the effect of the CRY2 destabilization has diverged among  
307 different tissues (Hirano et al., 2013; Yoo et al., 2013). Collectively, we  
308 demonstrated that the A260T mutation destabilizes CRY2 proteins *in vivo*, likely  
309 through alteration of FBXL3-mediated CRY2 degradation, leading to

310 perturbation of the circadian clock.

311

## 312 **Discussion**

313 We report here a mutation in hCRY2 that causes FASP in humans. We initially  
314 identified this as a novel variant. Since that time, it has been recognized as a  
315 rare variant in the SNP database (rs201220841). The frequency of the A260T  
316 allele (0.00008 in the ExAc database) is much lower than that of FASP (0.5%,  
317 our unpublished data) in the general population. This is consistent with the  
318 A260T variant found in one of our FASP families being responsible for a small  
319 portion of FASP in the general population.

320         Among the mutation carriers of this family (Figure 1A), the proband, her  
321 twin sister, and her mother have clear advanced sleep phase. In contrast, the  
322 nephew of the proband (101374) did not have early sleep onset and offset  
323 although his genotype is A/G (Figure1-source data). Considering his age, we  
324 classified him as “unknown”, since adolescents and young adults are typically  
325 more difficult to categorize as having a definite circadian phenotype due to  
326 normal phase delays seen in many people beginning in adolescence and  
327 persisting into young adult life (boys/men > than girls/women) (Roenneberg et al.,  
328 2004). When phenotyped at age 21, subject 101374 was at the statistical peak  
329 age of maximum phase delay due to these developmental effects and was prone  
330 to be even more phase-delayed by his male sex. Therefore, he may become  
331 progressively more phase advanced as he grows older as a result of the CRY2

332 FASP allele as it is unmasked by these developmental changes. It is also  
333 possible that the mutation may not have 100% penetrance and therefore the  
334 nephew will never manifest the FASP trait.

335           In order to confirm that the A260T mutation is causative of FASP, we  
336 generated mice carrying the mutation and subjected them to detailed behavioral  
337 analysis (Figure 2). Consistent with the other FASP mutations previously  
338 reported (in *hCK1 $\delta$*  and *hPER3*, the effects of the human mutation observed in  
339 mouse models and *in vitro* are subtle compared to those found in forward  
340 mutagenesis screens. This is expected since the mutations that we identified are  
341 found in extant humans in the “real world”. The circadian body clock plays crucial  
342 roles in maintaining normal physiological functions. Thus, any mutation  
343 manifesting the strong phenotypes seen in mutagenesis screens would almost  
344 certainly have been a selective disadvantage if they arose spontaneously in  
345 humans. Furthermore, while the phase advance in mice carrying the human  
346 *PER2* mutation appears to be due largely to a shortening of circadian period, the  
347 published *PER3* mice and the *CRY2* mice reported here both have altered  
348 entrainment. We speculate that some of FASP in humans is caused by altered  
349 entrainment properties that would not have been detected in forward  
350 mutagenesis screens because they have focused almost entirely on measuring  
351 period (not phase) as the target phenotype.

352           Previously, we have used wheel-running behavior analysis to  
353 characterize mouse models carrying human FASP mutations (Xu et al., 2007;

354 2005). Here, we investigated an additional behavior analysis method. For the  
355 *hCRY2-A260T* mouse model, we also employed continuous video recording  
356 (Figure 2A and Figure 2-supplement 1). We found that video recording was quite  
357 sensitive to detect advanced sleep phase (Figure 2A-C and Figure  
358 2-supplement 1). Although wheel-running also displays the phase advance of  
359 activity offset in the *hCRY2-A260T* mice (Figure 2-supplement 2), the data from  
360 wheel-running is less robust for detecting a phase advance of activity onset. This  
361 is likely due to a strong light-masking effect for mouse at the light-to-dark  
362 transition for activity onset. Thus, when the lights are on, mice are less likely to  
363 run on a wheel. However, smaller amplitude movements like grooming behavior  
364 and moving in the cage were detected by video recording. Wheel running was  
365 quite sensitive to detect phase advance of activity offset as this is seen during  
366 the dark phase of LD 12:12.

367         In this study, we found that the circadian period was significantly  
368 shortened by the A260T mutation in the central and peripheral clocks (Figure 2F,  
369 3A-E). Growing evidence indicates that stability of CRY proteins dominantly  
370 determines the circadian period length (Godinho et al., 2007; Hirano et al., 2014;  
371 Shi et al., 2013; Siepka et al., 2007; St John et al., 2014): stabilization of CRY  
372 lengthens circadian period in mice whereas destabilization of CRY shortens the  
373 period. Consistent with this model, our human mutation destabilizes CRY2 and  
374 leads to a short circadian period of mouse behavioral rhythms (Figure 6F).  
375 Shortened circadian periods have been measured in one FASP human subject

376 (Jones et al., 1999), and in mouse models of human FASP mutations (Xu et al.,  
377 2007; 2005). Mutant animals having a shorter free-running period such as *tau*  
378 mutant hamster also tend to exhibit advanced phase of behavioral rhythms in LD  
379 (Lowrey et al., 2000). Thus, it is likely that the *CRY2* mutation results in FASP, at  
380 least in part, through shortening of the free-running period.

381         Interestingly, our data also indicates that another circadian clock feature,  
382 phase resetting by light, is dysregulated in the h*CRY2* mutant mouse model.  
383 h*CRY2-A260T* mice have a smaller phase-shift in response to a light pulse in  
384 early subjective night compared to h*CRY2-WT* mice (Figure 2E; Figure  
385 2-supplement 3). In order to live on a 24 hour day in LD 12:12, wild-type mice  
386 need to phase delay a small amount each day because the endogenous  
387 circadian period is slightly shorter than 24 hours. A reduced ability to  
388 phase-delay observed in the h*CRY2-A260T* mouse model could contribute to  
389 advanced sleep phase, though the mechanism for the altered phase-shift  
390 remains to be elucidated. Although the difference in the free-running period of  
391 the transgenic mice was subtle as compared to the degree of phase-advance  
392 manifested in human mutation carriers or mice carrying the mutant h*PER2*  
393 transgene (Figure 2B, F), it is reasonable to expect that the alteration of both  
394 circadian period and light-induced phase-shifting together will strongly influence  
395 the phase angle of entrainment. The *after-hours* mutation in the mouse *Fbxl3*  
396 gene causes stabilization of CRY leading to an extremely long circadian period  
397 (Godinho et al., 2007). These mutant mice also exhibit large phase-shifts in

398 response to light (Guilding et al., 2013). The authors speculated that reduced  
399 amplitude of the circadian clock in *after-hours* mutant mice leads to the abnormal  
400 enhancement of phase-resetting. In this study, the A260T mutation elevated  
401 PER1 and PER2 levels, especially at ZT14, and the amplitude of PER1 protein  
402 rhythm was greater in hCRY2-A260T vs. hCRY2-WT mice (Figure 6D). Thus, the  
403 effect of light pulses in the early night may be decreased by the perturbed  
404 protein profiles (increased amplitude) of PER1 and PER2 in hCRY2-A260T  
405 mice.

406 FAD is a chromophore binding to flavo proteins regulating various  
407 biological processes and it is required for the light-sensing activity of CRY in  
408 various species (Lin and Todo, 2005; Partch and Sancar, 2005). *Drosophila*  
409 CRY is degraded by the proteasome in response to light signals, which is a  
410 trigger for phase-resetting of the circadian clock in flies. However, the ability of  
411 mammalian CRYs as a photoreceptor remains controversial as double knockout  
412 mice of *Cry1* and *Cry2* are still able to entrain to light and show *Per1* gene  
413 induction in SCN in response to light pulses (Okamura et al., 1999). These  
414 double knockout mice completely lack behavioral rhythms in constant darkness  
415 (van der Horst et al., 1999). Furthermore, the repressor activity of CRY on  
416 E-boxes and its interaction with other clock proteins are independent of light  
417 (Griffin et al., 1999). These findings emphasize the light-independent role of  
418 CRY proteins in mammals. Thus, the physiological role of FAD binding in the  
419 mammalian clock has been totally unknown, while a previous study implied that

420 FAD can structurally compete with FBXL3. Our findings provide the first  
421 evidence that FAD functions as a stabilizer of CRY2 protein by modulating  
422 FBXL3-CRY2 interaction (Figure 5). The results presented here demonstrate  
423 that the protein stability of CRY2 regulated by the balance of FBXL3 and FAD  
424 controls clock speed and sleep/wake timing in mice and humans.

425         Several genetic studies reported that the human *CRY2* gene is  
426 associated with mood regulation, cancer and glucose homeostasis (Dupuis et al.,  
427 2010; Hoffman et al., 2010; Kovanen et al., 2013; Lavebratt et al., 2010; Sjöholm  
428 et al., 2010; Zhang et al., 2013). Although psychiatric disorders, cancer, and  
429 metabolic disorders are tightly connected with dysfunction of the biological clock,  
430 associations of *CRY2* polymorphisms with morning/evening preference or other  
431 circadian phenotypes have not been described. One polymorphism in the  
432 *FBXL3* gene was reported to be associated with diurnal preference (Parsons et  
433 al., 2014), implying the conserved role of *FBXL3* in the human circadian clock.  
434 However, it remains to be elucidated whether that variant in *FBXL3* is causative  
435 (vs. merely be associated with) the human circadian phenotype and whether it  
436 acts through *CRY* regulation. Here, we demonstrate that regulatory mechanisms  
437 for *CRY2* protein are well conserved between mice and humans and that control  
438 of *CRY2* stability is critical for appropriate phase angle and period of the  
439 circadian clock in humans.

440

441

442 **Material and Methods**

443 **Method Summary**

444 All human subjects signed a consent form approved by the Institutional Review  
445 Boards at the University of Utah and the University of California, San Francisco  
446 (IRB# 10-03952). The consent form includes all confidentiality and ethic  
447 guidelines and also indicates not revealing subject information in the publication.  
448 All experimental protocols (Protocol no. AN111686-02) were conducted  
449 according to US National Institutes of Health guidelines for animal research and  
450 were approved by the Institutional Animal Care and Use Committee at the  
451 University of California, San Francisco.

452

453 **Human data and mutation screening**

454 Subjects were characterized by a previously published procedure established by  
455 one of the authors (CRJ, Jones et al., 1999). The data were interpreted by one of  
456 the authors (CRJ) as possible, probable, definite, or severe advanced sleep  
457 phase syndrome by at least age 30. Though ancillary features of ASP (earlier  
458 spontaneous wake time if an earlier bed time is selected) and potential  
459 confounding or masking influences were considered, most participants  
460 categorized as “definite ASP” reported spontaneous vacation sleep onset and  
461 offset time no later than 21:30 and 05:30, respectively and had H-O score (or  
462 numerically equivalent childhood MEQ score) of at least 72. We considered  
463 children and adolescents more difficult to categorize as having a definite,

464 life-long circadian phenotype unless it was severe by all measures including  
465 DLMO phase. DNAs purified from blood samples were used to screen for  
466 mutations.

467 The salivary dim light melatonin onset (DLMO) of the proband was obtained on  
468 the last night of the home recordings. DLMO phase was assessed from serial  
469 saliva samples (~1 mL) collected at 30 minutes intervals using “Salivette” saliva  
470 collection tubes (Sarstedt, Inc., Newton, NC) in dim light ( $\leq 10$  lux) confirmed  
471 by recording the ambient light level before each sample using a luxmeter  
472 (Sinometer, ShenZhen, China). Samples were collected, beginning 6 hours  
473 before the subject's typical bedtime. Saliva samples were frozen overnight and  
474 then shipped the next day in an insulated box with frozen coolant to another  
475 laboratory (Solid Phase, Portland, Maine) for radioimmunoassay by test kit  
476 (APLOCO Diagnostics, Windham, NH). The lower limit of detection of this assay  
477 is 0.2 pg/mL. The salivary dim light melatonin onset (DLMO) in adults was  
478 calculated and compared with a population sample not purposely selected for  
479 morning or evening preference by the method and data of Burgess and Fogg  
480 (Burgess and Fogg, 2008). Concurrent sleep logs and Zeo (Zeo Incorporated,  
481 Newton, Massachusetts) EEG recordings were obtained for ten consecutive  
482 nights of sleep at home. DNAs purified from blood samples were used to screen  
483 for mutations. For this particular family, a list of candidate genes including  
484 *CLOCK*, *BMAL1*, *PER1-3*, *CRY1-2*, *DEC1-2*, *CSNK1D*, *CSNK1E*, *PRKAA2*,  
485 *NPAS2*, *CSNK2A2*, *CSNK2B*, *FBXL3*, *GSK3B*, *PKCA*, *PRKAA1*, *PRKAA2*,

486 *RAB3A*, *RORA*, *TIMELESS*, *NR1D1*, and *PRKCG* were screened. *CRY2*  
487 (Accession number; EAW68030) A260T was identified as a novel variant  
488 specific for mutation carriers of this family (at the time of identification in 2008).  
489 The prevalence of the A260T allele (rs201220841) is 0.008% and 0.1% in the  
490 two sets of public genome databases, of which sample sizes are 121,412 and  
491 1,323, respectively.

492

#### 493 **Engineering of BAC constructs for generating transgenic mice**

494 A human BAC RP11-1084E2 containing the entire *CRY2* gene on a 189 kb  
495 genomic insert was obtained from CHORI (Children's Hospital Oakland  
496 Research Institute). The BAC clone was modified by homologous recombination  
497 using the Counter-Selection BAC Modification Kit (Gene Bridges GmbH) as  
498 previously described (Lee et al., 2012). Briefly, a linear PCR fragment  
499 containing a streptomycin/kanamycin counter selection gene was amplified. The  
500 primers for this reaction were designed so that 20 nucleotides would anneal to  
501 the streptomycin/kanamycin gene and an additional 40 nucleotides homologous  
502 to sequences flanking the mutation site. This PCR product was transferred into  
503 the RP11-1084E2 BAC to initiate homologous recombination in the DH10B  
504 *Escherichia coli* strain that already contained the plasmid pSC101- BAD-gbaA<sup>tet</sup>.  
505 The counter selection gene was then removed by a second recombination event  
506 using an oligonucleotide carrying the mutation (G-to-A) in the center. All relevant  
507 segments generated by PCR and recombination were sequence confirmed.

508 Detailed mapping was carried out for the modified BACs to ensure that correct  
509 constructs were obtained. Transgenic mice were generated using standard  
510 microinjection procedures. The transgenic founders were on a C57BL/6 × SJL F<sub>1</sub>  
511 background and were backcrossed to C57BL/6 mice in successive generations.  
512 The copy number for each transgenic line was calculated by quantitative  
513 real-time PCR using common sequences for mouse *Cry2* (reference) and  
514 human *CRY2* genes.

515

#### 516 **Purchased mouse lines**

517 *mPer2<sup>Luc</sup>* knockin mice (RRID IMSR\_006852) and *mCry2* knockout mouse  
518 (RRID IMSR\_016185) were purchased from The Jackson Laboratory and  
519 crossed with h*CRY2* transgenic mice.

520

#### 521 **Wheel-running analysis of transgenic mice**

522 All mice tested were ~8 week-old males maintained on a C57BL/6J background.  
523 Mice were kept in individual wheel running cages with free access to food and  
524 water. First, mice were entrained to LD 12:12. Activity profiles, offset time and  
525 acrophase were analyzed using data from day 10 to day 14 in LD. After  
526 entrainment to LD for approximately 3 weeks, mice were released into constant  
527 darkness (DD) for measurement of free-running period. Circadian periods were  
528 calculated by line fitting of activity onsets from day 7 to day 19 in DD. To analyze  
529 for phase-shifts, mice were given a 30 min-light pulse (200 lux) beginning at

530 ZT14 (2 hours after lights-off) or at ZT22 (2 hours before lights-on), and then  
531 released into DD. Phase-shifts were determined by line fitting of activity onsets  
532 from day1 to day7 in DD. All data collection and analysis was done using  
533 ClockLab software (Actimetrics, Wilmette, IL; RRID SCR\_014309). Activity onset  
534 and offset were defined using the ClockLab software algorithm. The default  
535 template is 6 hours of inactivity followed by 6 hours activity for onset (or vice  
536 versa for offset).

537

#### 538 **ANY-maze analysis of transgenic mice**

539 All mice tested were ~16 week-old males maintained on a C57BL/6J background.  
540 Mice were kept in individual cages with free access to food and water. Mice were  
541 monitored by infrared camera and tracked by an automatic video tracking  
542 system (Storling, Wood Dale, IL; RRID SCR\_014289). Mice were entrained to  
543 LD 12:12 for 1 week and then locomotor activity was recorded for 3 or 4 days.  
544 Walking distance and immobility times were calculated using ANY-maze  
545 software and data were averaged. Samples with over 500-meter walking  
546 distance or below 10,000-sec immobility time each day were excluded from the  
547 statistical analysis due to the failure of automatic tracking.

548

#### 549 **Cell culture and constructs**

550 HEK293 cells (ATCC CRL-1573; RRID CVCL\_0045) and NIH 3T3 cells (ATCC  
551 CRL-1658; RRID CVCL\_0594) were purchased from ATTC. Authentication of

552 the cell lines was performed using STR profiling by ATCC. Mycoplasma  
553 contamination was checked every 6 months and mycoplasma-free cell lines  
554 were used for all experiments in this study. Cells were cultured in DMEM (Sigma  
555 Aldrich) containing 10% FBS and 100 U/ml Penicillin-Streptomycin (Life  
556 Technologies) and maintained by standard methods. Mouse embryonic  
557 fibroblasts (MEFs) were prepared from E12.5 embryos of *hCRY2-WT* and  
558 *hCRY2-A260T* transgenic mice. After removing the head, paws and internal  
559 organs, embryos were chopped and incubated in 0.25% trypsin in PBS for 24 hr  
560 at 4°C. After incubation for 20 min at 37°C in 0.25% trypsin in PBS, cells were  
561 dissociated by pipetting in DMEM. Supernatant was cultured in a cell culture dish  
562 with DMEM and maintained by standard methods. Cells were transfected with  
563 Lipofectamine 3000 transfection reagent (Life Technologies) according to  
564 manufacturer's protocol. DNA constructs used for transfections are as follows:  
565 *hCRY2-WT-Myc-His/pcDNA3.1*, *hCRY2-A260T-Myc-His/pcDNA3.1*,  
566 *hCRY2-A260D-Myc-His/pcDNA3.1*, *hCRY2-WT-HA/pCMV-tag2B*,  
567 *hCRY2-A260T-HA/pCMV-tag2B*, *FLAG-hCRY2-WT/p3×FLAG-CMV-10*,  
568 *FLAG-hCRY2-A260T/p3×FLAG-CMV-10*, *FLAG-hCRY1-WT/p3×FLAG-CMV-10*,  
569 *FLAG-hCRY1-A241T/p3×FLAG-CMV-10*, *FLAG-hFBXL3/p3×FLAG-CMV-10*,  
570 *FLAG-hBMAL1/p3×FLAG-CMV-10*, *FLAG-hCLOCK/p3×FLAG-CMV-10*,  
571 *hCRY2-WT-LUC/p3×FLAG-CMV-10*, *hCRY2-A260T-LUC/p3×FLAG-CMV-10*,  
572 *hCRY2-A260D-LUC/p3×FLAG-CMV-10*, *mPer1-luc/pGL3*, pRL-TK (Renilla luc  
573 expression for internal control in luciferase assay, Promega).

574 0.3kb-*mBmal1*-luc/pGL3 is a gift by Dr.Yoshitaka Fukada (University of Tokyo).  
575 Mutant hCRY2 and hCRY1 expression vectors were generated by PCR-based  
576 site-directed mutagenesis, and the mutation was verified by sequencing. For  
577 knockdown of human *FBXL3*, Hs\_FBXL3\_1, Hs\_FBXL3\_2 FlexiTube siRNA  
578 (QIAGEN) and control siRNA (QIAGEN) were purchased.

579

#### 580 **Bioluminescence rhythms in tissue culture**

581 hCRY2 transgenic mice were crossed with *mPer2<sup>Luc</sup>* knock-in mice (Yoo et al.,  
582 2004; RRID IMSR\_JAX006852). Mice were sacrificed between ZT11 and ZT12.  
583 Dissected liver tissues were cultured on Millcell culture membrane  
584 (PICMORG50, Millpore) in 35 mm dishes. For recording of lung rhythms,  
585 dissected lung tissue was placed in 35 mm dishes without Millcell culture  
586 membrane. Recording medium was phenol-red free DMEM (Sigma Aldrich)  
587 containing 10mM HEPES-pH7.0, 3.5g/L D-glucose, 0.2 mM luciferin potassium  
588 salt, 0.35 g/L sodium bicarbonate, 2% B-27 supplement (Life Technologies), 50  
589 U/ml penicillin-streptomycin (Life Technologies). Bioluminescence was  
590 continuously recorded in a LumiCycle 32 instrument (Actimetrics, Wilmette, IL).  
591 Bioluminescence was detrended by subtracting 24-hr average of  
592 bioluminescence using the LumiCycle analysis software. The periods were  
593 determined by dampened sine-curve fitting using LumiCycle analysis.

594

#### 595 **Bioluminescence rhythms in cell culture**

596 For hCRY2 transgenic/mCry2 knockout MEFs and NIH3T3 stable cells, cells  
597 were transfected with 500 ng 0.3kbp-m*Bmal1*-luc/pGL3 by Lipofectamine3000  
598 before recordings. Cellular rhythms were synchronized by treatment with 100 nM  
599 dexamethasone (DEX) for 2 hours. Medium was changed to the recording  
600 medium: phenol-red free DMEM (Sigma Aldrich) containing 10mM  
601 HEPES-pH7.0, 3.5g/L D-glucose, 0.1 mM luciferin potassium salt and 50 U/ml  
602 penicillin-streptomycin (Life Technology). Bioluminescence recording and data  
603 analysis were as described in the methods for “Bioluminescence rhythms in  
604 tissue culture”.

605

#### 606 **Luciferase assay**

607 HEK293 cells were transfected with 50 ng *Per1*-luc expression vector, 25 ng  
608 Renilla luc control vector and 2, 5, 10 or 20 ng hCRY2 expression vectors. The  
609 luciferase assay was performed with Dual-Luciferase Reporter Assay System  
610 (Promega) according to the manufacturer’s protocol. Bioluminescence was  
611 detected by Synergy™ H4 Hybrid Multi-Mode Microplate Reader (BioTek).  
612 Bioluminescence of Firefly LUC was normalized to bioluminescence of Renilla  
613 LUC.

614

#### 615 **Luciferase-based degradation assay**

616 The hCRY2-LUC fusion protein expressing vector was created by inserting a  
617 *CRY2-Luc* cDNA between EcoRI and BamHI sites in the p3×FLAG-CMV-10

618 vector. HEK293 cells were transfected with 50 ng hCRY2-LUC vectors and  
619 cultured for 24 hours. The culture medium was replaced with recording  
620 medium [phenol-red free DMEM (Sigma Aldrich) supplemented with 10% fetal  
621 bovine serum, 3.5 mg/ml glucose, 50 U/ml penicillin-streptomycin (Life  
622 Technologies), 0.05 mM luciferin, and 10 mM HEPES-NaOH; pH 7.0] containing  
623 100 µg/ml cycloheximide (CHX; Santa Cruz Biotechnology Inc.). Luciferase  
624 activity of hCRY2-LUC was recorded at 10-min intervals at 37°C with a  
625 LumiCycle 32 instrument (Actimetrics). The luminescence signals were fitted to  
626 an exponential function to quantify the half-life of CRY2-LUC. KL001 (Cayman  
627 Chemical) was diluted in DMSO to a final concentration of 20 mM.

628

### 629 **Expression profiles of proteins and genes**

630 Mice were entrained to LD 12:12 for at least 10 days. Mice were transferred to  
631 DD, and mice were sacrificed in dim red light on the 2nd day of DD. Liver tissues  
632 were collected, followed by nuclear extraction (Yoshitane et al., 2009) and  
633 mRNA extraction. Protein levels and mRNA levels were normalized to LaminB  
634 levels and *Gapdh* levels, respectively.

635

### 636 **Western Blotting**

637 For whole-cell extracts, HEK293 cells were lysed in SDS sample buffer [62.5mM  
638 Tris-HCl (pH 6.8), 50mM DTT, 2% SDS, 10% glycerol]. Preparation of the  
639 cytosolic and the nuclear fractions of mouse liver was performed as previously

640 described (Yoshitane et al., 2009). Protein samples were separated by  
641 SDS-PAGE. Tissues were transferred to PVDF membranes (Millipore) with  
642 blocking in T-TBS [50mM Tris-HCl (pH 7.4), 137mM NaCl, 0.1% Tween 20]  
643 containing 1% Skim milk. Primary antibodies were reacted in the blocking  
644 solution at 4°C overnight. Then, secondary antibodies were reacted in the  
645 blocking solution at RT for 2 hr. Proteins were detected with the Western  
646 Lightning Plus ECL (PerkinElmer). Band intensities were determined using  
647 Image J software.  $\beta$ -actin and Vinculin were used as loading controls for total  
648 cell lysates, and LaminB and TBP were used as nuclear markers. Proteins were  
649 detected with the following antibodies: anti-cMyc 9E10 (Santa Cruz, sc-40),  
650 anti-FLAG M2 (Sigma Aldrich, F1804), anti-HA Y11 (Santa Cruz, sc-805-G),  
651 anti- $\beta$ -actin (Abcam, AC-15), anti-Vinculin (Abcam, ab18058), anti-TBP (Santa  
652 Cruz, sc-273), anti-Ub (Santa Cruz, sc-8017), anti-hPER1 (Thermo Scientific,  
653 PA1-524), anti-LaminB1 (Abcam, ab16048 and Santa Cruz, C20), anti-mPER2  
654 (Alpha Diagnostic International, PER-21A), anti-hCRY2 (Santa Cruz, sc-130731)  
655 and anti-mCRY1 (MBL, PM081). Rabbit polyclonal anti-mCRY2 antibody was  
656 provide by Dr.Yoshitaka Fukada (University of Tokyo)(Hirano et al., 2013).  
657 Secondary antibodies used were goat anti-mouse IgG-HRP (Santa Cruz,  
658 sc-2005), goat anti-rabbit IgG-HRP (Santa Cruz, sc-2006) and goat anti-guinea  
659 pig IgG-HRP (Santa Cruz, sc2438).

660

661 **FAD competition assay**

662 Flavin adenine dinucleotide disodium salt hydrate (FAD, Sigma Aldrich) was  
663 diluted in PBS to a final concentration of 100 mM. HEK293 cells were  
664 transfected with plasmid vectors for 10 µg hCRY2-His-Myc (WT or A260T) and  
665 10 µg FLAG-hFBXL3. Forty-two hours after transfection, the cells were treated  
666 with 10 µM MG132 (Calbiochem) for 6 hours. CRY2-FBXL3 complex was  
667 purified with anti-FLAG M2 affinity gel (Sigma Aldrich). FAD was incubated with  
668 CRY2-FBXL3 complex binding to anti-FLAG M2 affinity gel in 40 µl PBS for 2  
669 hours on ice. After centrifugation, the supernatant was collected as the 'released  
670 CRY2' sample. CRY2 still binding to FLAG-FBXL3 was eluted by adding SDS  
671 sample buffer to FLAG-M2 affinity gel.

672

### 673 **Immunoprecipitation**

674 HEK293 cells were transfected with plasmid vectors for hCRY2-His-Myc (WT or  
675 A260T) and FLAG-hFBXL3. Forty-two hours after transfection, the cells were  
676 treated with 10 µM MG132 (Calbiochem) for 6 hours. CRY2-FBXL3 complex  
677 was purified with anti-FLAG M2 affinity gel (Sigma Aldrich) and eluted by 300  
678 µg/ml 3×FLAG peptide (Sigma Aldrich).

679

### 680 **Real-time qPCR**

681 Total RNA was extracted by TRIzol reagent (Life Technologies) from MEFs or  
682 liver samples of transgenic animals. cDNA was synthesized by Superscript III  
683 (Life Technologies) for MEFs or GoScript (Promega) for liver samples.

684 Quantification of mRNA was performed with GoTaq Real-Time qPCR Kits  
685 (Promega) using gene specific primers. mRNA levels were normalized to mouse  
686 *Gapdh* levels.  
687 Primers: mouse *Per1*-fw; CAGGCTAACCAGGAATATTACCAGC,  
688 mouse *Per1*-rv; CACAGCCACAGAGAAGGTGTCCTGG,  
689 mouse *Per2*-fw; ATGCTCGCCATCCACAAGA,  
690 mouse *Per2*-rv; GCGGAATCGAATGGGAGAAT,  
691 mouse *Gapdh*-fw; ACGGGAAGCTCACTGGCATGGCCTT,  
692 mouse *Gapdh*-rv; CATGAGGTCCACCACCCTGTTGCTG,  
693 mouse *Cry2*-fw; GGGACTCTGTCTATTGGCATCTG,  
694 mouse *Cry2*-rv; GTCACTCTAGCCCGCTTGGT,  
695 mouse *Cry1*-fw:CCCAGGCTTTTCAAGGAATGGAACA  
696 mouse *Cry1*-rv:TCTCATCATGGTCATCAGACAGAGG  
697 human *CRY2*-fw; CCAAGAGGGAAGGGCAGGGTAGAG,  
698 human *CRY2*-rv; AGGATTTGAGGCACTGTTCCGAGG  
699 mouse *Dbp* FW,AATGACCTTTGAACCTGATCCCGCT  
700 mouse *Dbp* RV,GCTCCAGTACTTCTCATCCTTCTGT  
701 mouse *Bmal1* FW,GCAGTGCCACTGACTACCAAGA  
702 mouse *Bmal1* RV,TCCTGGACATTGCATTGCAT  
703 mouse *Rev-erb $\alpha$*  FW,GGGCACAAGCAACATTACCA  
704 mouse *Rev-erb $\alpha$*  RV,CACGTCCCCACACACCTTAC  
705 mouse *REV-erb $\beta$*  FW,TGGGACTTTTGAGGTTTTAATGG

706 mouse *REV-erbβ* RV,GTGACAGTCCGTTCTTTGC  
707 mouse *Dec1* FW,ATCAGCCTCCTTTTTGCCTTC  
708 mouse *Dec1* RV,AGCATTCTCCAGCATAGGCAG  
709 mouse *Dec2* FW,ATTGCTTTACAGAATGGGGAGCG  
710 mouse *Dec2* RV,AAAGCGCGCGAGGTATTGCAAGAC

711

### 712 **Structural modeling**

713 Structural modeling was based on the structure of mouse CRY2 bound to FAD  
714 (PDB code 4I6G) and mouse FBXL3 (PDB code 4I6J)(Xing et al., 2013).  
715 Modeling of mutant CRY2 was performed using Molecular graphics and  
716 analyses were performed with the UCSF Chimera package (RRID  
717 SCR\_004097). Chimera was developed by the Resource for Biocomputing,  
718 Visualization, and Informatics at the University of California, San Francisco  
719 (supported by NIGMS P41-GM103311)(Pettersen et al., 2004).

720

### 721 **Statistics analysis**

722 All error bars in the figures represent SEM except for Figure 3C. In Figure 3C,  
723 the error bars represent SD. No statistical analysis was used to predetermine the  
724 sample sizes. Experiments were not randomized and not analyzed blindly. In  
725 Figure 2A and Figure 2-supplement 1, the sample with extremely abnormal  
726 walking distance (>500 meter walking distance, due to a failure of automatic  
727 video tracking) was excluded as an outlier according to the Smirnov-Grubbs test.

728 Data was statistically analyzed using R software (RRID SCR\_001905). To  
729 assess statistical significance, data was obtained from three or more  
730 independent experiments. All data sets were assumed to follow normal  
731 distributions by the Kolmogorov-Smirnov test, and homogeneity of variance  
732 between compared groups was tested by F-test (comparison of 2 groups) or  
733 Bartlett test (comparison of multiple groups). Two-tailed paired Student's *t*-test or  
734 Welch's *t*-test was used for the comparison of 2 groups with or without  
735 homogeneity of variance. Tukey's test or Games-Howell test were used for  
736 multiple comparisons with or without of homogeneity of variance. Differences  
737 with a *P* value <0.05 were considered statistically significant.

738

### 739 **Acknowledgements**

740 This work was funded by NIH grant GM079180 and HL059596 to L.J.P. and  
741 Y-H.F and by the William Bowes Neurogenetics Fund. The initial sequencing and  
742 analysis were performed at Lawrence Berkeley National Laboratory and at the  
743 United States Department of Energy Joint Genome Institute (Department of  
744 Energy Contract DE-AC02-05CH11231, University of California). The authors  
745 wish to thank Drs. Philip Kurien and Pei-Ken Hsu and Mr. David Wu for  
746 suggestions and critical reading of the manuscript. We thank Dr. Yoshitaka  
747 Fukada (University of Tokyo) for providing anti-CRY2 antibody and 0.3  
748 kbp-*mBmal1*-luc construct. L.J.P. is an investigator of the Howard Hughes  
749 Medical Institute. A.H. was supported by the Japanese Society for the Promotion

750 of Science (JSPS) and the Uehara Memorial Foundation (Japan).

751

## 752 **Additional Information**

## 753 **Author Contributions**

754 C.R.J carried out human circadian evaluations. A.L. and L.A.P. performed initial  
755 genomic sequencing and analysis. G.S. and Y. X. generated the BAC transgenic  
756 mouse models. W.C.H. performed structural modeling. A.H., T.M. and M.Y.  
757 performed experiments. A.H, Y.-H.F, and L.J.P designed experiments, analyzed  
758 data and wrote the manuscript.

759

## 760 **References**

761 Burgess, H.J., and Fogg, L.F. (2008). Individual differences in the amount and  
762 timing of salivary melatonin secretion. *PLoS ONE* 3, e3055.

763 Busino, L., Bassermann, F., Maiolica, A., Lee, C., Nolan, P.M., Godinho, S.I.,  
764 Draetta, G.F., and Pagano, M. (2007). SCFFbx13 controls the oscillation of the  
765 circadian clock by directing the degradation of cryptochrome proteins. *Science*  
766 316, 900–904.

767 Czarna, A., Berndt, A., Singh, H.R., Grudziecki, A., Ladurner, A.G., Timinszky,  
768 G., Kramer, A., and Wolf, E. (2013). Structures of Drosophila Cryptochrome and  
769 Mouse Cryptochrome1 Provide Insight into Circadian Function. *Cell* 153, 1394–  
770 1405.

771 Dupuis, J., Langenberg, C., Prokopenko, I., Saxena, R., Soranzo, N., Jackson,  
772 A.U., Wheeler, E., Glazer, N.L., Bouatia-Naji, N., Gloyn, A.L., et al. (2010). New  
773 genetic loci implicated in fasting glucose homeostasis and their impact on type 2  
774 diabetes risk. *Nat Genet* 42, 105–116.

775 Godinho, S.I.H., Maywood, E.S., Shaw, L., Tucci, V., Barnard, A.R., Busino, L.,  
776 Pagano, M., Kendall, R., Quwailid, M.M., Romero, M.R., et al. (2007). The  
777 after-hours mutant reveals a role for Fbxl3 in determining mammalian circadian  
778 period. *Science* 316, 897–900.

779 Griffin, E.A., Staknis, D., and Weitz, C.J. (1999). Light-independent role of CRY1  
780 and CRY2 in the mammalian circadian clock. *Science* 286, 768–771.

781 Guilding, C., Scott, F., Bechtold, D.A., Brown, T.M., Wegner, S., and Piggins,  
782 H.D. (2013). Suppressed cellular oscillations in after-hours mutant mice are  
783 associated with enhanced circadian phase-resetting. *The Journal of Physiology*  
784 591, 1063–1080.

785 He, Y., Jones, C.R., Fujiki, N., Xu, Y., Guo, B., Holder, J.L., Rossner, M.J.,  
786 Nishino, S., and Fu, Y.H. (2009). The Transcriptional Repressor DEC2  
787 Regulates Sleep Length in Mammals. *Science* 325, 866–870.

788 Hirano, A., Kurabayashi, N., Nakagawa, T., Shioi, G., Todo, T., Hirota, T., and  
789 Fukada, Y. (2014). In Vivo Role of Phosphorylation of Cryptochrome 2 in the  
790 Mouse Circadian Clock. *Molecular and Cellular Biology* 34, 4464–4473.

791 Hirano, A., Yumimoto, K., Tsunematsu, R., Matsumoto, M., Oyama, M.,  
792 Kozuka-Hata, H., Nakagawa, T., Lanjakornsiripan, D., Nakayama, K.I., and  
793 Fukada, Y. (2013). FBXL21 Regulates Oscillation of the Circadian Clock through  
794 Ubiquitination and Stabilization of Cryptochromes. *Cell* 152, 1106–1118.

795 Hirota, T., Lee, J.W., St John, P.C., Sawa, M., Iwaisako, K., Noguchi, T.,  
796 Pongsawakul, P.Y., Sonntag, T., Welsh, D.K., Brenner, D.A., et al. (2012).  
797 Identification of Small Molecule Activators of Cryptochrome. *Science* 337, 1094–  
798 1097.

799 Hitomi, K., DiTacchio, L., Arvai, A.S., Yamamoto, J., Kim, S.-T., Todo, T., Tainer,  
800 J.A., Iwai, S., Panda, S., and Getzoff, E.D. (2009). Functional motifs in the (6-4)  
801 photolyase crystal structure make a comparative framework for DNA repair

802 photolyases and clock cryptochromes. *Proc Natl Acad Sci U S a.* 106, 6962–  
803 6967.

804 Hoffman, A.E., Zheng, T., Yi, C.H., Stevens, R.G., Ba, Y., Zhang, Y., Leaderer,  
805 D., Holford, T., Hansen, J., and Zhu, Y. (2010). The Core Circadian Gene  
806 Cryptochrome 2 Influences Breast Cancer Risk, Possibly by Mediating Hormone  
807 Signaling. *Cancer Prevention Research* 3, 539–548.

808 Jones, C.R., Campbell, S.S., Zone, S.E., Cooper, F., DeSano, A., Murphy, P.J.,  
809 Jones, B., Czajkowski, L., and Ptáček, L.J. (1999). Familial advanced  
810 sleep-phase syndrome: A short-period circadian rhythm variant in humans.  
811 *Nature Medicine* 5, 1062–1065.

812 Kaasik, K., Kivimäe, S., Allen, J.J., Chalkley, R.J., Huang, Y., Baer, K., Kissel, H.,  
813 Burlingame, A.L., Shokat, K.M., Ptáček, L.J., et al. (2013). Glucose Sensor  
814 O-GlcNAcylation Coordinates with Phosphorylation to Regulate Circadian Clock.  
815 *Cell Metabolism* 17, 291–302.

816 Kovanen, L., Kaunisto, M., Donner, K., Saarikoski, S.T., and Partonen, T. (2013).  
817 CRY2 genetic variants associate with dysthymia. *PLoS ONE* 8, e71450.

818 Kume, K., Zylka, M.J., Sriram, S., Shearman, L.P., Weaver, D.R., Jin, X.,  
819 Maywood, E.S., Hastings, M.H., and Reppert, S.M. (1999). mCRY1 and mCRY2  
820 Are Essential Components of the Negative Limb of the Circadian Clock  
821 Feedback Loop. *Cell* 98, 193–205.

822 Lavebratt, C., Sjöholm, L.K., Soronen, P., Paunio, T., Vawter, M.P., Bunney,  
823 W.E., Adolfsson, R., Forsell, Y., Wu, J.C., Kelsoe, J.R., et al. (2010). CRY2 is  
824 associated with depression. *PLoS ONE* 5, e9407.

825 Lee, H.-Y., Nakayama, J., Xu, Y., Fan, X., Karouani, M., Shen, Y., Pothos, E.N.,  
826 Hess, E.J., Fu, Y.-H., Edwards, R.H., et al. (2012). Dopamine dysregulation in a  
827 mouse model of paroxysmal nonkinesigenic dyskinesia. *J. Clin. Invest.* 122,  
828 507–518.

829 Lin, C., and Todo, T. (2005). The cryptochromes. *Genome Biol.* 6, 220.

830 Lowrey, P.L., and Takahashi, J.S. (2004). Mammalian circadian biology:  
831 elucidating genome-wide levels of temporal organization. *Annu Rev Genomics*  
832 *Hum Genet* 5, 407–441.

833 Lowrey, P.L., Shimomura, K., Antoch, M.P., Yamazaki, S., Zemenides, P.D.,  
834 Ralph, M.R., Menaker, M., and Takahashi, J.S. (2000). Positional syntenic  
835 cloning and functional characterization of the mammalian circadian mutation tau.  
836 *Science* 288, 483–491.

837 Nangle, S., Xing, W., and Zheng, N. (2013). Crystal structure of mammalian  
838 cryptochrome in complex with a small molecule competitor of its ubiquitin ligase.  
839 *Cell Research* 23, 1417–1419.

840 Okamura, H., Okamura, H., Miyake, S., Sumi, Y., Yamaguchi, S., Yasui, A.,  
841 Muijtjens, M., Hoeijmakers, J.H.J., and van der Horst, G.T.J. (1999). Photic  
842 induction of mPer1 and mPer2 in Cry-Deficient Mice Lacking a Biological Clock.  
843 *Science* 286, 2531–2534.

844 Parsons, M.J., Lester, K.J., Barclay, N.L., Archer, S.N., Nolan, P.M., Eley, T.C.,  
845 and Gregory, A.M. (2014). Polymorphisms in the circadian expressed genes  
846 PER3 and ARNTL2 are associated with diurnal preference and GNβ3 with sleep  
847 measures. *J Sleep Res* 23, 595–604.

848 Partch, C.L., and Sancar, A. (2005). Cryptochromes and Circadian  
849 Photoreception in Animals. *Methods in Enzymology* 393, 726–745.

850 Pettersen, E.F., Goddard, T.D., Huang, C.C., Couch, G.S., Greenblatt, D.M.,  
851 Meng, E.C., and Ferrin, T.E. (2004). UCSF Chimera--a visualization system for  
852 exploratory research and analysis. *J Comput Chem* 25, 1605–1612.

853 Reid, K.J., and Burgess, H.J. (2005). Circadian Rhythm Sleep Disorders.  
854 *Primary Care: Clinics in Office Practice* 32, 449–473.

855 Reid, K.J., Chang, A.-M., Dubocovich, M.L., Turek, F.W., Takahashi, J.S., and  
856 Zee, P.C. (2001). Familial advanced sleep phase syndrome. *Arch Neurol* 58,  
857 1089–1094.

858 Reischl, S., and Kramer, A. (2011). Kinases and phosphatases in the  
859 mammalian circadian clock. *FEBS Letters* 585, 1393–1399.

860 Reppert, S.M., and Weaver, D.R. (2001). MOLECULAR ANALYSIS OF  
861 MAMMALIAN CIRCADIAN RHYTHMS. *Annu. Rev. Physiol* 63, 647–676.

862 Roenneberg, T., Kuehnle, T., Pramstaller, P.P., Ricken, J., Havel, M., Guth, A.,  
863 and Mewes, M. (2004). A marker for the end of adolescence. *Curr Biol* 14,  
864 R1038–R1039.

865 Sanada, K., Harada, Y., Sakai, M., Todo, T., and Fukada, Y. (2004). Serine  
866 phosphorylation of mCRY1 and mCRY2 by mitogen-activated protein kinase.  
867 *Genes Cells* 9, 697–708.

868 Shearman, L.P., Sriram, S., Weaver, D.R., Maywood, E.S., Chaves, I., Zheng,  
869 B., Kume, K., Lee, C.C., Hastings, M.H., and Reppert, S.M. (2000). Interacting  
870 molecular loops in the mammalian circadian clock. *Science* 288, 1013–1019.

871 Shi, G., Xing, L., Liu, Z., Qu, Z., Wu, X., Dong, Z., Wang, X., Gao, X., Huang, M.,  
872 Yan, J., et al. (2013). Dual roles of FBXL3 in the mammalian circadian feedback  
873 loops are important for period determination and robustness of the clock. *Proc*  
874 *Natl Acad Sci U S a.* 110, 4750–4755.

875 Siepka, S.M., Yoo, S.-H., Park, J., Song, W., Kumar, V., Hu, Y., Lee, C., and  
876 Takahashi, J.S. (2007). Circadian mutant Overtime reveals F-box protein FBXL3  
877 regulation of cryptochrome and period gene expression. *Cell* 129, 1011–1023.

878 Sjöholm, L.K., Backlund, L., Cheteh, E.H., Ek, I.R., Frisén, L., Schalling, M.,  
879 Osby, U., Lavebratt, C., and Nikamo, P. (2010). CRY2 is associated with rapid  
880 cycling in bipolar disorder patients. *PLoS ONE* 5, e12632.

881 St John, P.C., Hirota, T., Kay, S.A., and Doyle, F.J. (2014). Spatiotemporal  
882 separation of PER and CRY posttranslational regulation in the mammalian  
883 circadian clock. *Proc Natl Acad Sci U S a.* 111, 2040–2045.

884 Stojkovic, K., Wing, S.S., and Cermakian, N. (2014). A central role for  
885 ubiquitination within a circadian clock protein modification code. *Front Mol*  
886 *Neurosci* 7, 69.

887 Takahashi, J.S. (1995). Molecular neurobiology and genetics of circadian  
888 rhythms in mammals. *Annu. Rev. Neurosci.* 18, 531–553.

889 Toh, K.L., Jones, C.R., He, Y., Eide, E.J., Hinz, W.A., Virshup, D.M., Ptáček, L.J.,  
890 and Fu, Y.-H. (2001). An hPer2 phosphorylation site mutation in familial  
891 advanced sleep phase syndrome. *Science* 291, 1040–1043.

892 van der Horst, G.T.J., Muijtjens, M., Kobayashi, K., Takano, R., Kanno, S.-I.,  
893 Takao, M., de Wit, J., Verkerk, A., Eker, A.P.M., van Leenen, D., et al. (1999).  
894 Mammalian Cry1 and Cry2 are essential for maintenance of circadian rhythms.  
895 *Nature* 398, 627–630.

896 Vitaterna, M.H., Selby, C.P., Todo, T., Niwa, H., Thompson, C., Fruechte, E.M.,  
897 Hitomi, K., Thresher, R.J., Ishikawa, T., Miyazaki, J., et al. (1999). Differential  
898 regulation of mammalian period genes and circadian rhythmicity by  
899 cryptochromes 1 and 2. *Proc. Natl. Acad. Sci. U.S.a.* 96, 12114–12119.

900 Xing, W., Busino, L., Hinds, T.R., Marionni, S.T., Saifee, N.H., Bush, M.F.,  
901 Pagano, M., and Zheng, N. (2013). SCFFBXL3 ubiquitin ligase targets  
902 cryptochromes at their cofactor pocket. *Nature* 496, 64–68.

903 Xu, Y., Toh, K.L., Jones, C.R., Shin, J.Y., Fu, Y.H., and Ptáček, L.J. (2007).  
904 Modeling of a Human Circadian Mutation Yields Insights into Clock Regulation  
905 by PER2. *Cell* 128, 59–70.

906 Xu, Y., Padiath, Q.S., Shapiro, R.E., Jones, C.R., Wu, S.C., Saigoh, N., Saigoh,  
907 K., Ptáček, L.J., and Fu, Y.-H. (2005). Functional consequences of a CK1delta  
908 mutation causing familial advanced sleep phase syndrome. *Nature* 434, 640–  
909 644.

910 Yoo, S.-H., Mohawk, J.A., Siepk, S.M., Shan, Y., Huh, S.K., Hong, H.-K.,  
911 Kornblum, I., Kumar, V., Koike, N., Xu, M., et al. (2013). Competing E3 ubiquitin

912 ligases govern circadian periodicity by degradation of CRY in nucleus and  
913 cytoplasm. *Cell* 152, 1091–1105.

914 Yoo, S.-H., Yamazaki, S., Lowrey, P.L., Shimomura, K., Ko, C.H., Buhr, E.D.,  
915 Siepka, S.M., Hong, H.-K., Oh, W.J., Yoo, O.J., et al. (2004).  
916 PERIOD2::LUCIFERASE real-time reporting of circadian dynamics reveals  
917 persistent circadian oscillations in mouse peripheral tissues. *Proc. Natl. Acad.*  
918 *Sci. U.S.a.* 101, 5339–5346.

919 Yoshitane, H., Takao, T., Satomi, Y., Du, N.H., Okano, T., and Fukada, Y.  
920 (2009). Roles of CLOCK Phosphorylation in Suppression of E-Box-Dependent  
921 Transcription. *Molecular and Cellular Biology* 29, 3675–3686.

922 Zhang, L., Hirano, A., Hsu, P.-K., Jones, C.R., Sakai, N., Okuro, M., McMahon,  
923 T., Yamazaki, M., Xu, Y., Saigoh, N., et al. (2016). A PERIOD3 variant causes a  
924 circadian phenotype and is associated with a seasonal mood trait. *Proc Natl*  
925 *Acad Sci U S a.* 113, E1536–E1544.

926 Zhang, L., Ptáček, L.J., and Fu, Y.-H. (2013). Diversity of Human Clock  
927 Genotypes and Consequences (Elsevier Inc.).

928

## 929 **Figure Legends**

### 930 **Figure 1. A CRY2 mutation in FASP kindred 50035.**

931 **(A)** Pedigree of the family (kindred 50035) segregating the CRY2 mutation  
932 (A260T). Circles and squares represent women and men, respectively. An  
933 asterisk marks the proband. A missense mutation from G to A causes an amino  
934 acid conversion from Alanine to Threonine at position 260. **(B)** Amino acid  
935 alignment around the mutation site. The A260T mutation is located in the  
936 N-terminal portion of the FAD binding domain in CRY2. This residue is highly

937 conserved among vertebrate species. CC denotes a Coiled-Coil sequence.

938

939 **Figure 2. hCRY2-A260T mice have advanced phase of sleep-wake**  
940 **behavior in a light-dark cycle and a shortened circadian period in constant**  
941 **darkness.**

942 **(A)** Mouse movement was tracked by an infrared video camera in LD. The ratio  
943 of immobilization time to total daily immobilization time (upper panel) and the  
944 ratio of walking distance to total daily distance (bottom panel) were plotted every  
945 10 min. Data are shown as means with SEM (n=8 for hCRY2-WT and  
946 hCRY2-A260T). **(B)** Peak time of immobility was measured by fitting a quadratic  
947 function to data from ZT0 to 13. Representative examples of curve fitting for  
948 hCRY2-WT and hCRY2-A260T are shown here. Data are shown as means with  
949 SEM (n=8 for hCRY2-WT and hCRY2-A260T, \*p<0.05 by Student's *t*-test). **(C)**  
950 Onset and offset of locomotor activity. Data are shown as means with SEM (n=8  
951 for hCRY2-WT and hCRY2-A260T). **(D)** Actograms of wheel-running activity for  
952 hCRY2-WT, hCRY2-A260T, and littermate transgene-negative mice. The blue  
953 shadows indicate periods when the lights were on. Red lines were fitted to  
954 activity onset using ClockLab analysis software. **(E)** Phase-shifts in response to  
955 a 30-min light exposure at ZT14 indicated by red arrows in **(D)**. \*p<0.05 by  
956 Tukey's test (n=7 for hCRY2-WT, n=11 for hCRY2-A260T, n=10 for WT). **(F)** The  
957 distribution of period measurements for BAC transgenic mice and transgene  
958 negative controls. Period was determined by line fitting of activity onset and

959 chi-square periodogram from day 7 to day 19 in DD. \* $p < 0.05$  (n=15 for  
960 hCRY2-WT, n=14 for hCRY2-A260T and n=7 for WT)

961

962 **Figure 3. Bioluminescence rhythms in tissue cultures from hCRY2-A260T**  
963 **mice and CRY2-A260T stable cell lines.**

964 (A) Representative rhythms of PER2::LUC bioluminescence in the liver and lung.

965 Data were detrended by subtracting the 24-hr average of bioluminescence. (B)

966 Period measurements of the bioluminescence rhythms in liver and lung tissues.

967 Data are shown as means  $\pm$  SEM (n=4 for liver and hCRY2-WT lung, n=3 for

968 hCRY2-A260T lung, \* $p < 0.05$  by Student's *t*-test). (C) Peak and trough time of

969 PER2::LUC bioluminescence rhythms of mouse liver and lung tissues. Data are

970 shown as means  $\pm$  SEM (n=4 for liver). Data are shown as means  $\pm$  SD (n=2 to

971 4 for lung, \* $p < 0.05$  by Student's *t*-test). (D) Representative rhythms of

972 PER2::LUC bioluminescence in MEFs from hCRY2 transgenic mice. Data were

973 detrended by subtracting the 24-hr average of bioluminescence. Period lengths

974 of the bioluminescence rhythms are shown as means  $\pm$  SEM (n=4, \* $p < 0.05$  by

975 Tukey's test). (E) Representative examples of bioluminescence rhythms of

976 *mBmal1-luc* in MEFs from transgenic mice on a *mCry2* knockout background.

977 Cells were transfected with *mBmal1-luc* vector 24 hours before the recording.

978 Data were detrended by subtracting the 24-hr average of bioluminescence.

979 Period lengths of the bioluminescence rhythms in the stable cell lines are shown

980 as means  $\pm$  SEM (n=4, \* $p < 0.05$  by Games-Howell test). (F) Representative

981 examples of bioluminescence rhythms of *Bmal1-luc* in NIH3T3 cells stably  
982 expressing FLAG-CRY2-WT or FLAG-CRY2-A260T. Data were detrended by  
983 subtracting the 24-hr average of bioluminescence. Period lengths of the  
984 bioluminescence rhythms in the stable cell lines are shown as means  $\pm$  SEM  
985 (n=3, \*p<0.05 by Student's *t*-test).

986

987 **Figure 4. CRY2-A260T is less stable, particularly in nuclei.**

988 **(A)** Luciferase activity driven by mouse *Per1* E-box in HEK293 cells. 2, 5, 10 and  
989 20 ng of hCRY2 expression vector (WT or A260T) was transfected into cells  
990 cultured in a 24-well plate. Luciferase activity was normalized to Renilla  
991 luciferase activity. Data are shown as means with SEM (n=4, \*p<0.05 by  
992 Student's *t*-test). **(B)** Protein levels of CRY2-WT and CRY2-A260T in the nuclear  
993 and cytosolic fractions of HEK293 cells. Data are shown as means with SEM  
994 (n=3, \*p<0.05 by Student's *t*-test). **(C)** Degradation assay of CRY2 protein in  
995 HEK293 cells. Forty-eight hours after transfection, cells were treated with 100  
996  $\mu$ g/ml CHX and fractionated into the nuclear and cytosolic fractions. CRY2  
997 protein levels at the starting point (t=0 hours) were normalized to 1. Data are  
998 shown as means with SEM (n=3\*, p<0.05 by Student's *t*-test).

999

1000 **Figure 5. CRY2-A260T binds more strongly to FBXL3 leading to faster**  
1001 **degradation of mutant CRY2.**

1002 **(A)** Effect of human *FBXL3* knockdown on CRY2 protein stability in HEK293

1003 cells. Forty-eight hours after transfection, the culture medium was changed to  
1004 the recording medium containing 100  $\mu\text{g/ml}$  CHX, and bioluminescence of  
1005 CRY2-LUC was recorded continuously. Bioluminescence normalized to the  
1006 value at time 0 was fitted to an exponential curve to determine half-life of  
1007 CRY2-LUC. Data are shown as means with SEM (n=4, \*p<0.05 by Welch's  
1008 *t*-test). **(B)** Effect of FAD on CRY2 protein levels. Forty-two hours after  
1009 transfection, HEK293 cells were treated with 100  $\mu\text{M}$  FAD for 6 hours. Data are  
1010 shown as means with SEM (n=3, \*p<0.05 by Student's *t*-test). **(C)** FAD and  
1011 FBXL3 competition assay. CRY2-FBXL3 complex expressed in HEK293 cells  
1012 was purified using FLAG antibody. FAD was added to CRY2-FBXL3 complex  
1013 and incubated at 4 °C for 2 hours *in vitro*. **(D)** CRY2 protein stability in the cells  
1014 treated with KL001. Twenty-four hours after transfection, the culture medium  
1015 was changed to the recording medium containing 100  $\mu\text{g/ml}$  CHX and KL001.  
1016 Recording of bioluminescence and calculation of half-life was performed as  
1017 described above. \*p<0.05 by Student's *t*-test (n=3). **(E)** Interaction of CRY2 with  
1018 FBXL3 in HEK293 cells treated with MG132 for 6 hours prior to harvesting. **(F)**  
1019 Ubiquitylation of CRY2. HEK293 cells expressing FLAG-CRY2 were treated with  
1020 MG132 for 6 hours before harvesting. FLAG-CRY2 was then purified and blotted  
1021 with anti-Ubiquitin antibody. Quantitative data are shown as means with SEM  
1022 (n=3, \*p<0.05 by Student's *t*-test).

1023

1024 **Figure 6. CRY2-A260T expression is down-regulated in hCRY2-A260T**

1025 **mice.**

1026 **(A)** CRY2 protein levels in synchronized MEFs. Cells were treated with 100 nM  
1027 Dex for 2 hours to synchronize the cellular rhythms. Media was change and  
1028 MEFs were cultured for 24 or 36 hours before harvesting. Quantified band  
1029 intensities of CRY2 (mouse CRY2 and human CRY2) are shown as means  $\pm$   
1030 SEM (n=3, \*p<0.05 by Student's *t*-test). **(B)** mRNA levels of clock genes in  
1031 synchronized MEFs. Cellular rhythms of MEFs were synchronized with 100 nM  
1032 Dex for 2 hours. mRNA levels were quantified by real-time PCR. Data are shown  
1033 as means  $\pm$  SEM (n=3, \*p<0.05 by Student's *t*-test). **(C)** Temporal expression  
1034 profiles of PER1, PER2, CRY1 and CRY2 in mouse liver. Mice were sacrificed  
1035 every 4 hours on the second day in DD. Asterisks mark non-specific bands. **(D)**  
1036 Quantification of protein levels in **(C)**. Data are shown as means  $\pm$  SEM (n=3).  
1037 **(E)** mRNA levels of indicated clock genes in mouse liver. Mice were sacrificed  
1038 every 4 hours on the second day in DD. mRNA levels of indicated genes were  
1039 quantified by real-time PCR using gene specific primers. Data are shown as  
1040 means  $\pm$  SEM (n=3). **(F)** Model of CRY2 protein regulation. In wild-type, FAD  
1041 binding to CRY2 acts to stabilize by competing with FBXL3. In hCRY2-A260T  
1042 transgenic mice or FASP human subjects with CRY2 mutations, FAD does not  
1043 protect CRY2 from FBXL3-mediated degradation. Destabilization of CRY2  
1044 results in shortened period, leading to advanced sleep phase. In *Fbxl3* knockout  
1045 mice or mutant mice (*Overtime* and *After-hours*)(Godinho et al., 2007; Siepka et  
1046 al., 2007), CRY2 is stabilized in the nucleus, thus lengthening the circadian

1047 period.

1048

1049 **Figure 1-source data 1**

1050 Summary of sleep phenotype of human subjects. Subject IDs correspondence to  
1051 numbers in Figure 1A.

1052

1053 **Figure 2-supplement 1**

1054 **(A)** CRY2 expression in total liver lysate at ZT18. CRY2 protein was detected by  
1055 human CRY2 antibody (Santa Cruz) and mouse CRY2 antibody (Hirano et al.,  
1056 2013). Copy number was determined by real-time PCR using common  
1057 sequences in mouse and human *Cry2* genes. **(B)** Representative profiles of  
1058 locomotor activity measured by video recording. Activity onset (black) and offset  
1059 (red) are indicated by arrows in the figures. The time of onset and offset for all  
1060 animals of respective genotypes are averaged and plotted in Figure2C. **(C)**  
1061 Locomotor activity and resting behavior of transgenic mice on a m*Cry2* knockout  
1062 background. Mouse movement was tracked by an infrared video camera in LD.  
1063 The ratio of immobilization time to total daily immobilization time (upper panel)  
1064 and the ratio of walking distance to total daily distance (bottom panel) were  
1065 plotted every 10 min. Data are shown as means with SEM (n=6 for  
1066 hCRY2-WT/*Cry2* KO, n=6 for hCRY2-A260T/*Cry2* KO). The average of activity  
1067 offset and onset in LD 12:12 are shown (n=6 for hCRY2-WT/*Cry2* KO, n=6 for  
1068 hCRY2-A260T/*Cry2* KO).

1069

1070 **Figure 2-supplement 2**

1071 (A) Activity profiles of transgenic mice in LD 12:12. Ratio of wheel-running  
1072 counts to total daily counts are plotted every 20 min (n=18 for hCRY2-WT, n=14  
1073 for hCRY2-A260T). The average of activity offset in LD 12:12 are shown in the  
1074 right graph. \*p<0.05 by Tukey's test (n=19 for hCRY2-WT, n=19 for  
1075 hCRY2-A260T and n=7 for WT). (B) Actograms and activity profiles of  
1076 transgenic mice on a mCry2 knockout background in LD 12:12. Ratio of  
1077 wheel-running counts to total daily counts are plotted every 5 min (n=5 for  
1078 hCRY2-WT, n=5 for hCRY2-A260T). The average of activity offset in LD 12:12  
1079 are shown in the right graph. \*p<0.05 by Tukey's test (n=5 for  
1080 hCRY2-WT/mCry2 KO, n=5 for hCRY2-A260T/mCry2 KO and n=6 for mCry2  
1081 KO).

1082

1083 **Figure 2-supplement 3**

1084 (A) Phase-shift in response to 30-min light exposure at ZT22. Mice were  
1085 exposed to a 30-min light pulse at ZT22 (indicated by red arrows) and released  
1086 into DD after the light pulse. The blue shadows indicate periods when the lights  
1087 were on. Red lines were fitted to activity onset using ClockLab analysis software.  
1088 Phase-shift was determined by line-fitting to activity onset (n=6 for hCRY2-WT,  
1089 n=7 for hCRY2-A260T and WT).

1090

1091 **Figure 2-supplement 4**

1092 (A) Circadian period of the transgenic mice on a *mCry2* knockout background.  
1093 Period was determined by chi-square periodogram from day 7 to day 14 in DD.  
1094 \* $p < 0.05$  by Welch's test ( $n=6$  for *hCRY2-WT/mCry2KO* and  $n=5$  for  
1095 *hCRY2-A260T/mCry2KO*). (B) Circadian period and phase-shift of  
1096 *hCRY2-A260T* mice line#2. Representative actograms of wheel-running activity  
1097 of *hCRY2-A260T* line#2 and littermate controls (*WT*) are shown. The blue  
1098 shadows indicate periods when the lights were on. Red lines were fitted to  
1099 activity onset using ClockLab analysis software. Phase-shifts shown here are by  
1100 30-min light exposure at ZT14 (left panel,  $n=7$  for *hCRY2-A260T* line#2,  $n=3$  for  
1101 *WT*). Period was determined by line fitting of activity onset from day 7 to day 19  
1102 in DD. \* $p < 0.05$  by Student's *t*-test (right panel,  $n=7$  for *hCRY2-A260T* line#2,  $n=3$   
1103 for *WT*).

1104

1105 **Figure 4-supplement 1**

1106 (A) Twenty-four hours after transfection, the culture media was changed to  
1107 recording media containing 100  $\mu\text{g/ml}$  CHX, and bioluminescence of CRY2-LUC  
1108 (*WT*, *A260T* or *A260D*) was recorded continuously. Bioluminescence normalized  
1109 to the start point was fitted to an exponential curve to determine half-life of  
1110 CRY2-LUC (right panel). Data are shown as means  $\pm$  SEM ( $n=4$ , \* $p < 0.05$  by  
1111 Tukey's test). Left panel shows representative bioluminescence decay of  
1112 CRY2-LUC. (B) Luciferase activity driven by mouse *Per1* E-box. 10 or 25 ng of

1113 *CRY2* construct was transfected to HEK293 cells cultured in 24-well plate.  
1114 Luciferase activity was normalized to Renilla luciferase activity. Data are shown  
1115 as means  $\pm$  SEM (n=3, \*p<0.05 by Tukey's test). **(C)** Degradation assay of *CRY1*  
1116 protein in HEK293 cells. Sixty hours after transfection, cells were treated with  
1117 100  $\mu$ g/ml CHX and fractionated into the nuclear and cytosolic fractions. *CRY1*  
1118 protein levels at the starting point (t=0 hours) were normalized to 1. Data are  
1119 shown as means with SEM (n=3\*, p<0.05 by Student's *t*-test).

1120

#### 1121 **Figure 5-supplement 1**

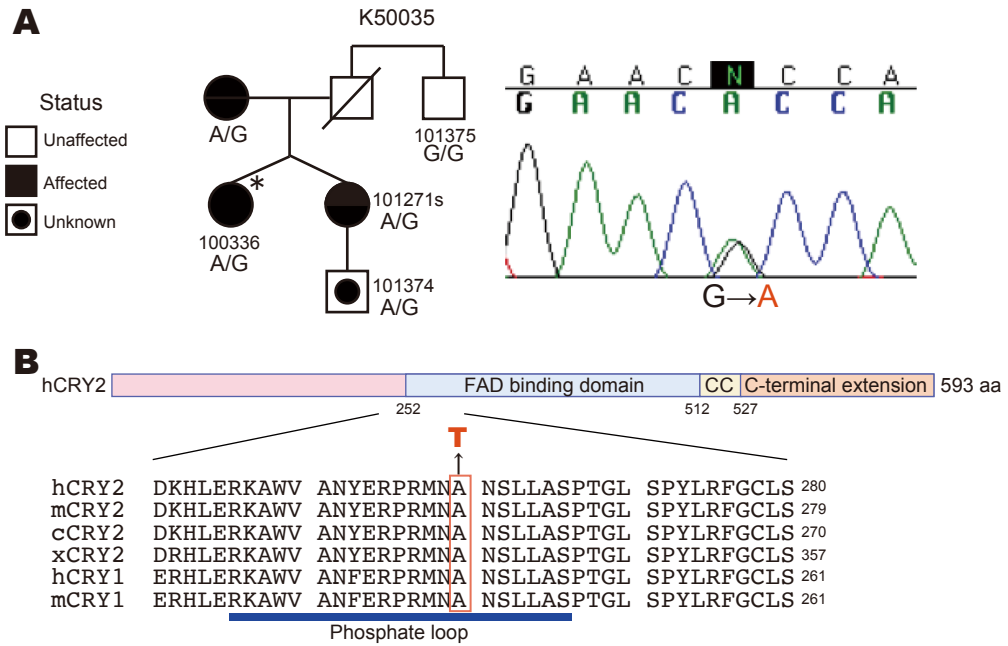
1122 **(A)** *CRY2* protein stability in the cells treated with KL001. Twenty-four hours after  
1123 transfection, the culture medium was changed to the recording medium  
1124 containing 100  $\mu$ g/ml CHX and KL001 at the indicated concentration. \*p<0.05 by  
1125 Student's *t*-test (n=3). **(B)** Structure of mouse *CRY2* bound to FAD (PDB code  
1126 4I6G) (orange) or FBXL3 (4I6J) (red). Green represents FBXL3. Short dashed  
1127 lines indicate the side chain of A259 (A260 of human *CRY2*). *CRY2* bound to  
1128 FBXL3 is in a more open conformation compared to the FAD-bound *CRY2*.

1129 **(C)** Structure of mouse *CRY2*-WT (top) or mouse *CRY2*-A259T (corresponded  
1130 to human *CRY2*-A260T, bottom) bound to FBXL3. The Ala to Thr mutation  
1131 increases the molecular density and likely changes the conformation of *CRY2*  
1132 from the FAD-bound form to the FBXL3-bound form, in which main chain around  
1133 A259 moved to left side in this image.

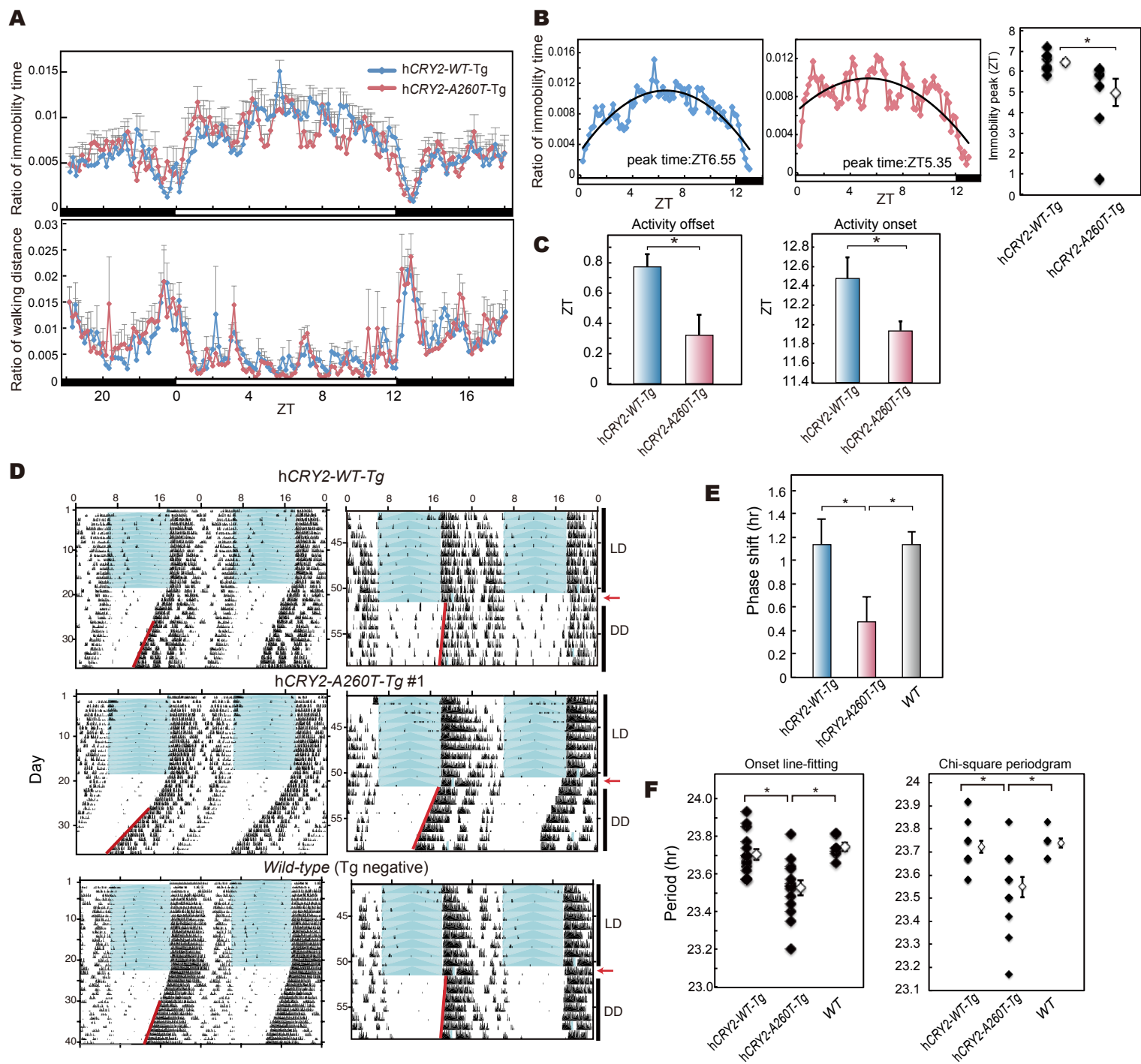
1134

1135 **Figure 6-supplement 1**

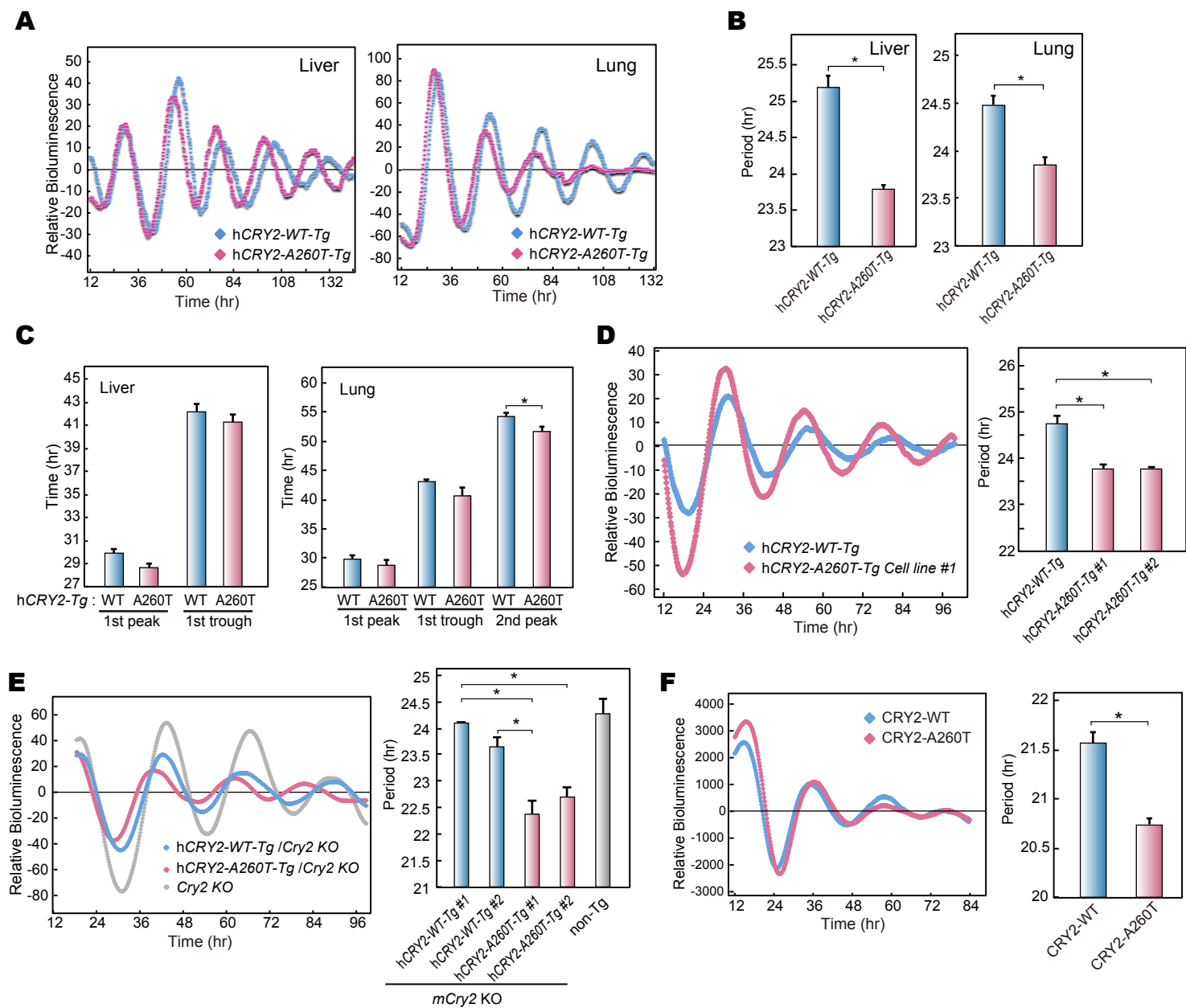
1136 **(A)** mRNA levels of indicated genes in synchronized MEFs. Cellular rhythms of  
1137 MEFs were synchronized with 100 nM Dex for 2 hours. mRNA levels were  
1138 quantified by real-time PCR. Data are shown as means  $\pm$  SEM (n=3, \*p<0.05 by  
1139 Student's *t*-test). **(B)** Expression patterns of indicated clock genes in mouse liver.  
1140 Mice were sacrificed every 4 hours on the second day in DD. mRNA levels of  
1141 indicated genes were quantified by real-time PCR using gene specific primers.  
1142 Data are shown as means  $\pm$  SEM (n=3).  
1143



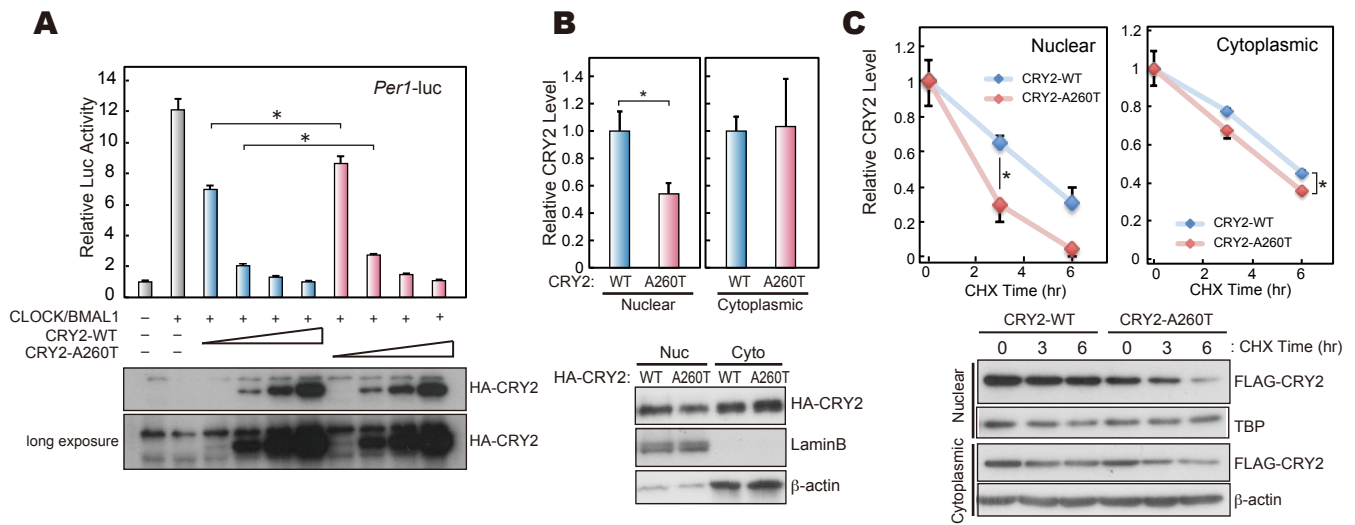
**Figure 1**



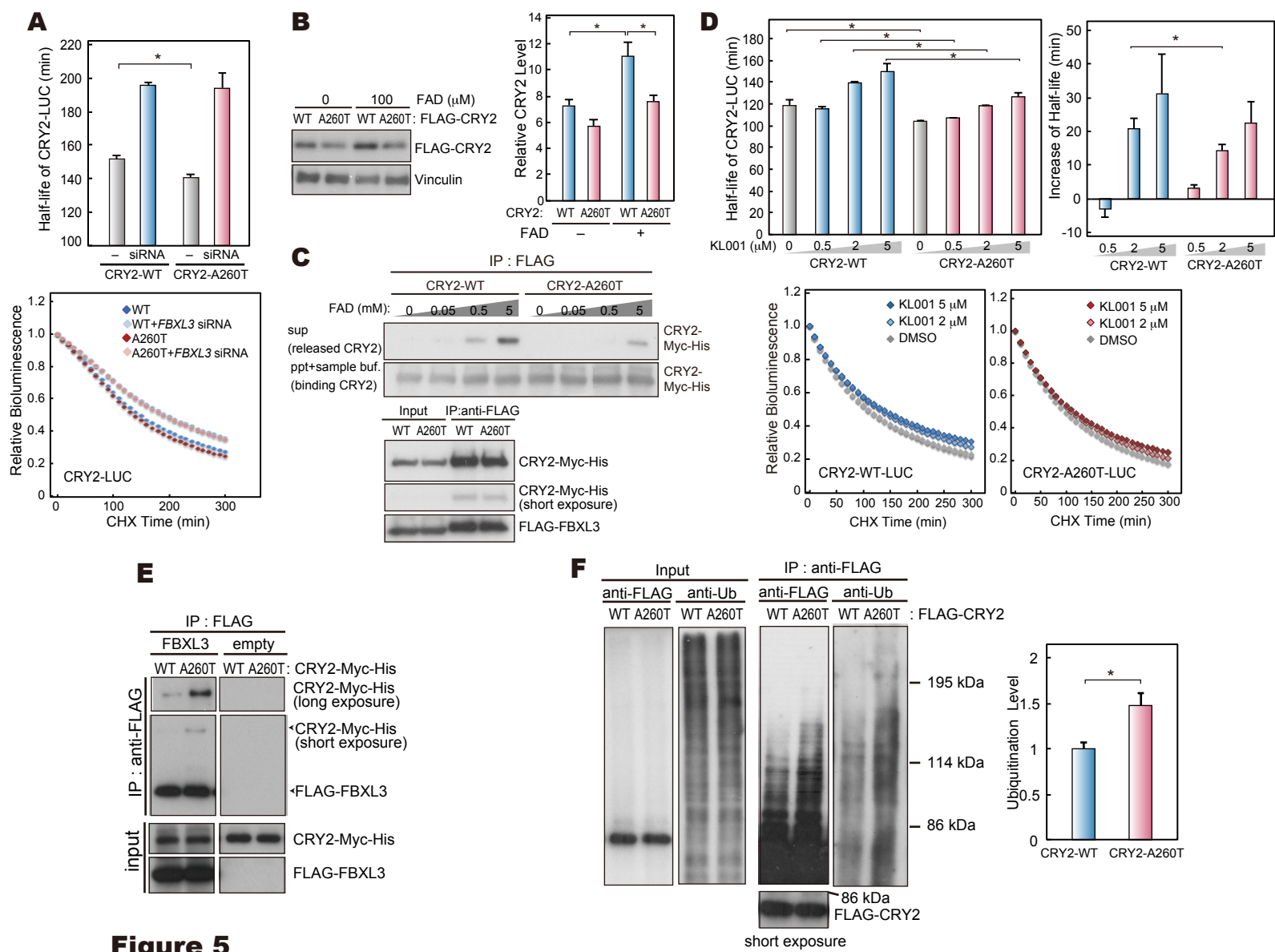
**Figure 2**



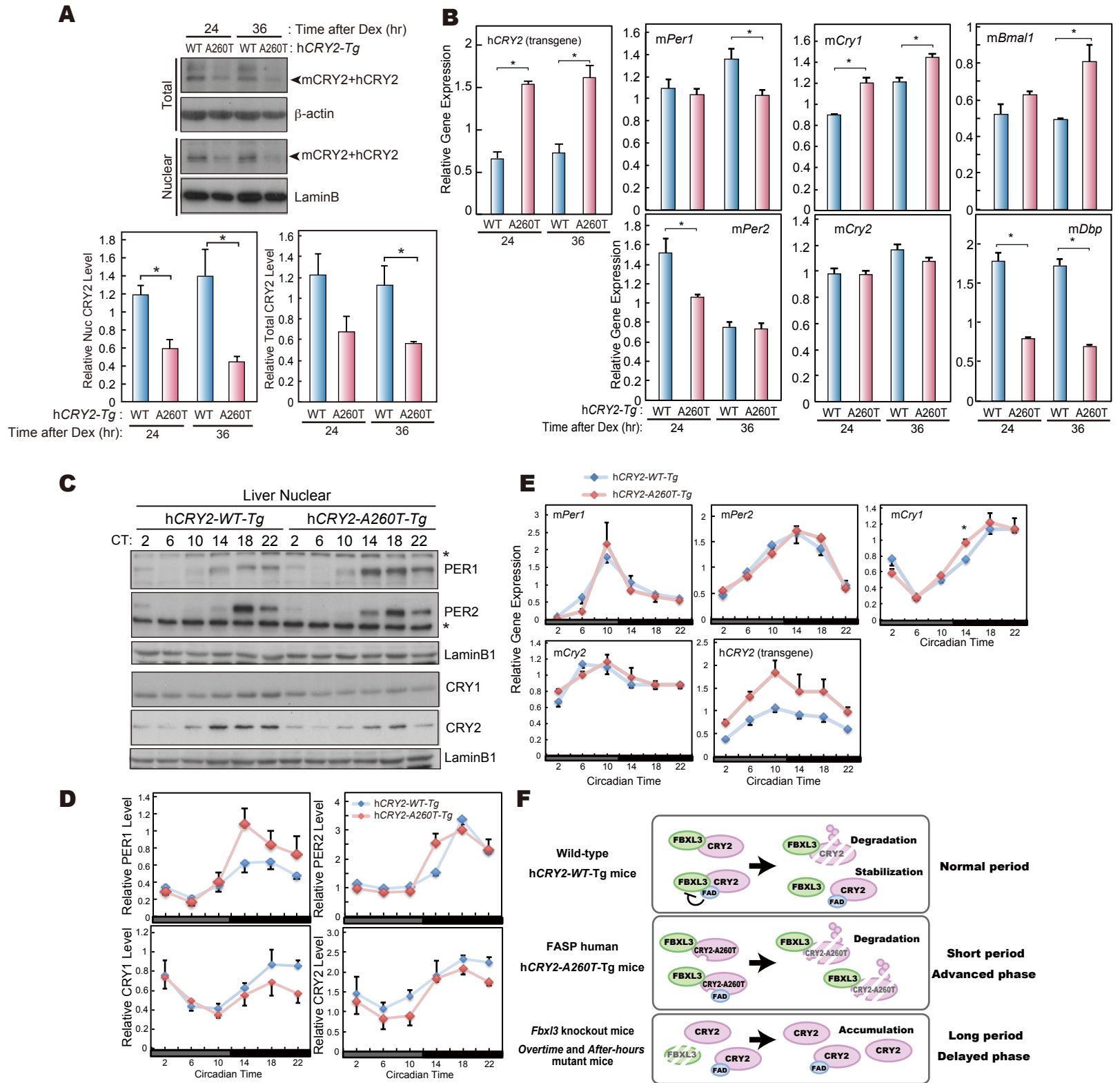
**Figure 3**



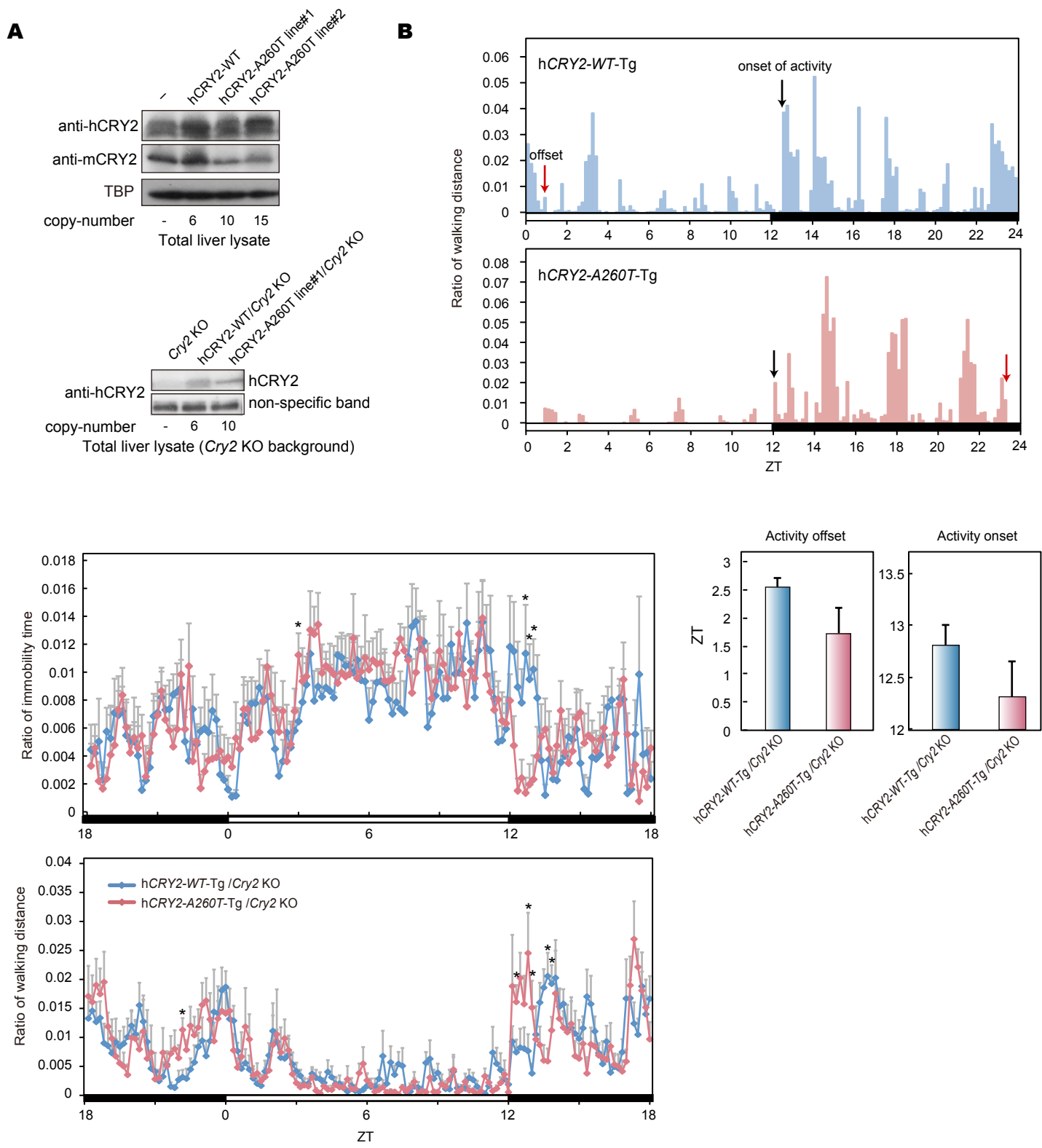
**Figure 4**



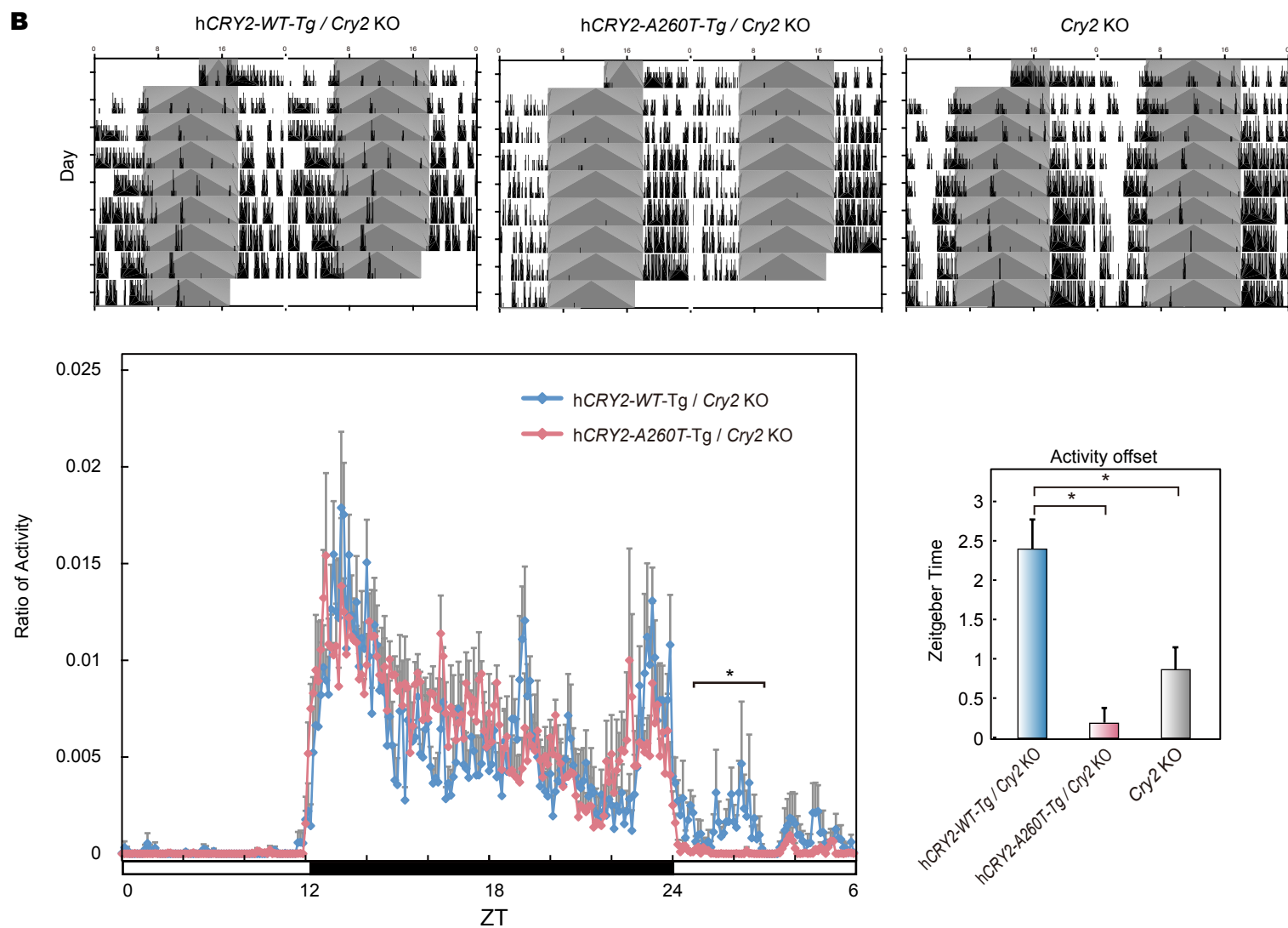
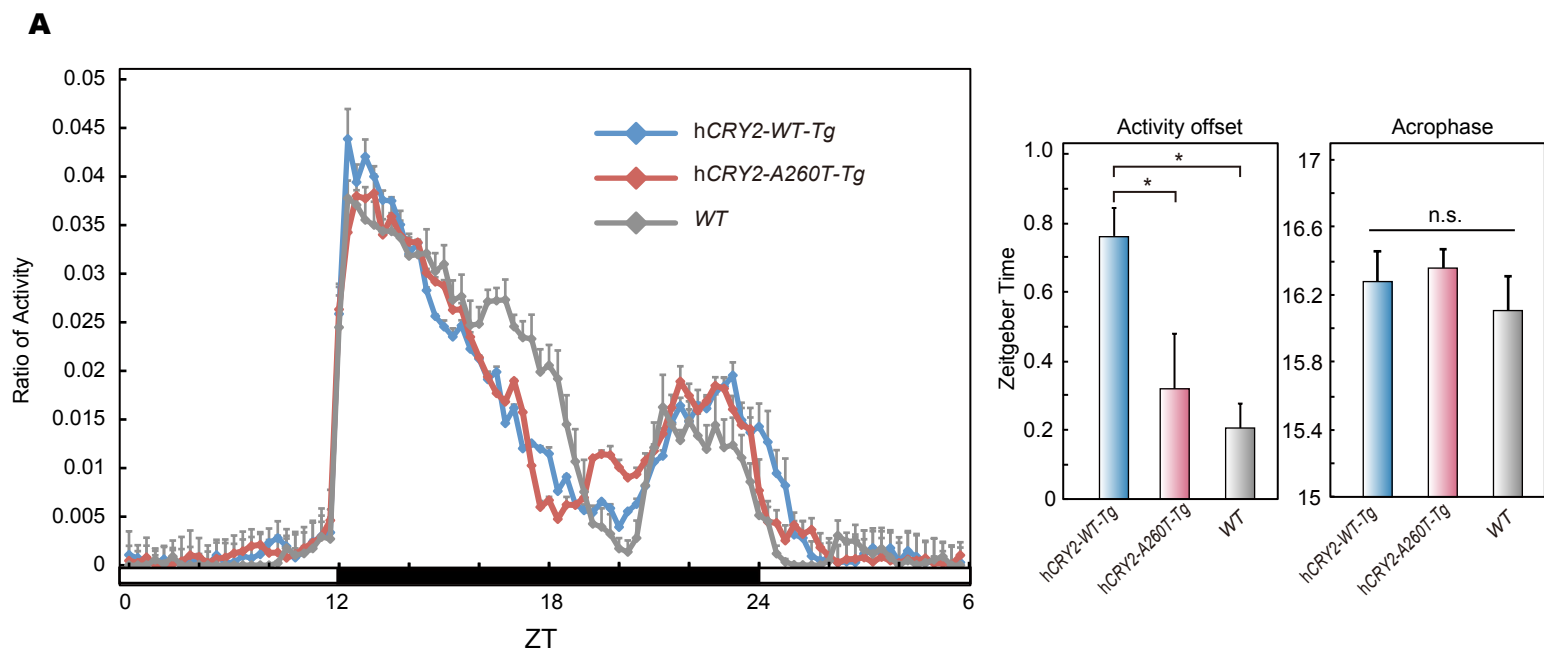
**Figure 5**



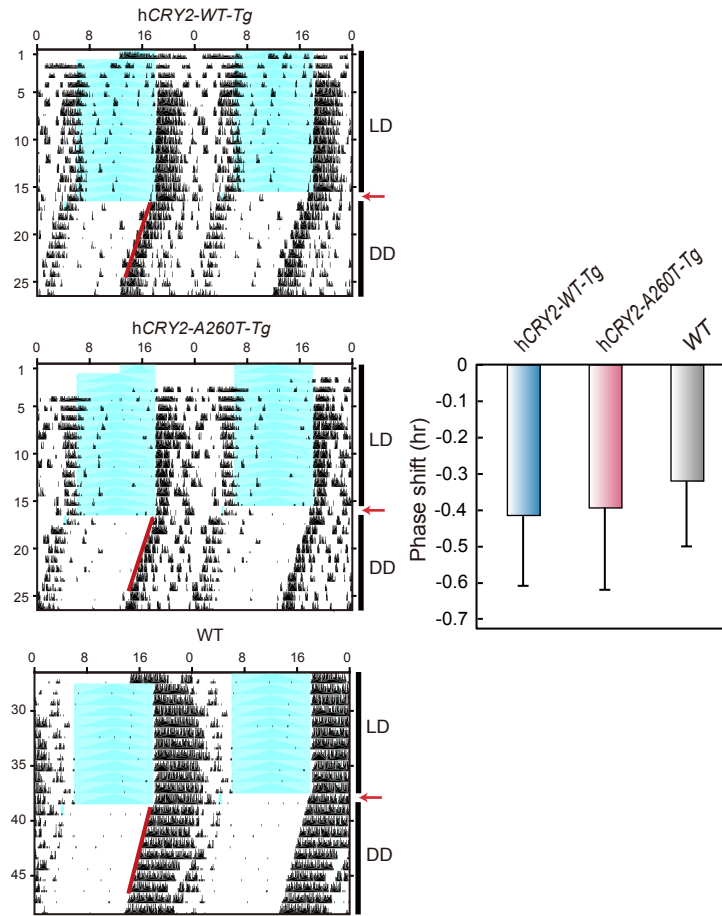
**Figure 6**



**Figure 2-Supplement 1**



**Figure 2-Supplement 2**

**A****Figure 2 - supplement 3**

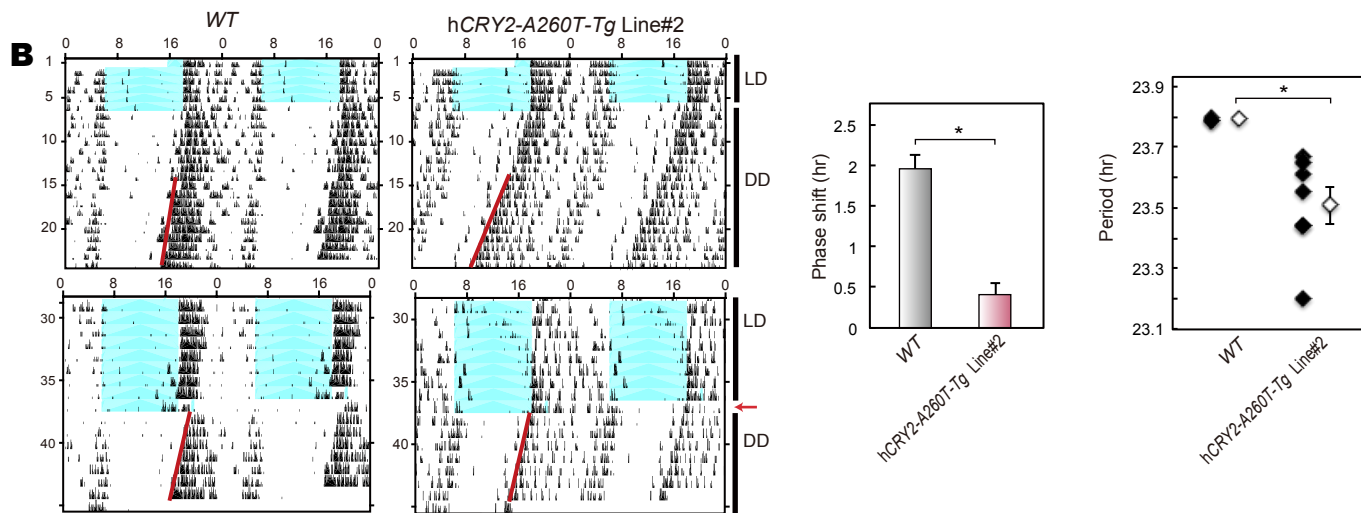
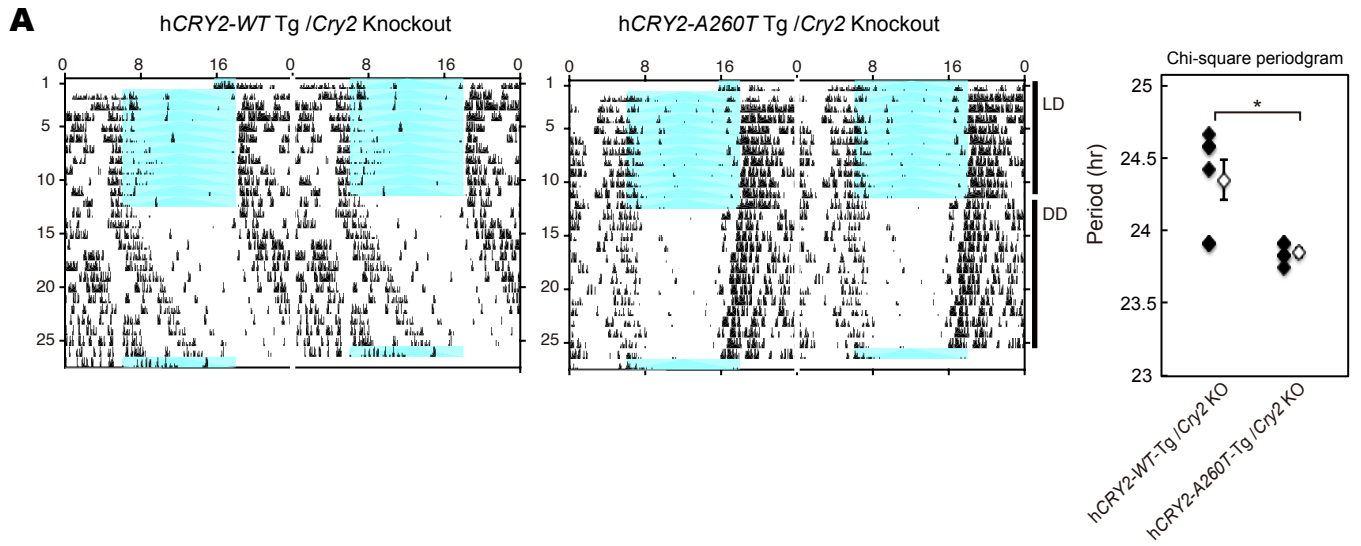


**Figure 2 - supplement 4**

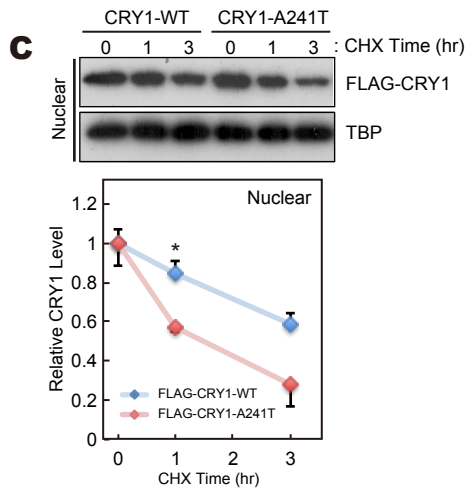
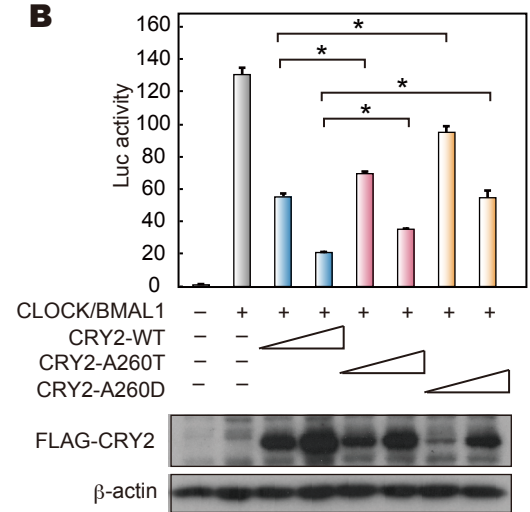
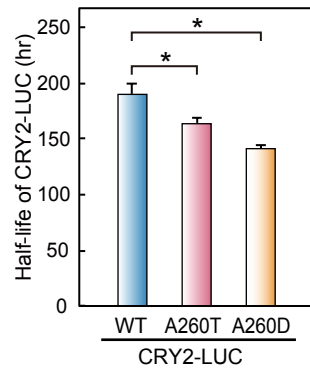
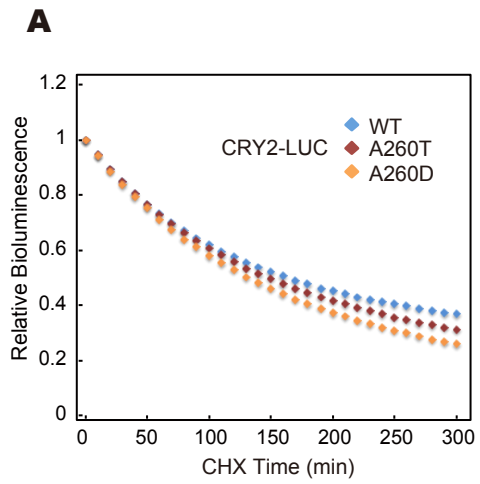


**Figure 4 - supplement 1**

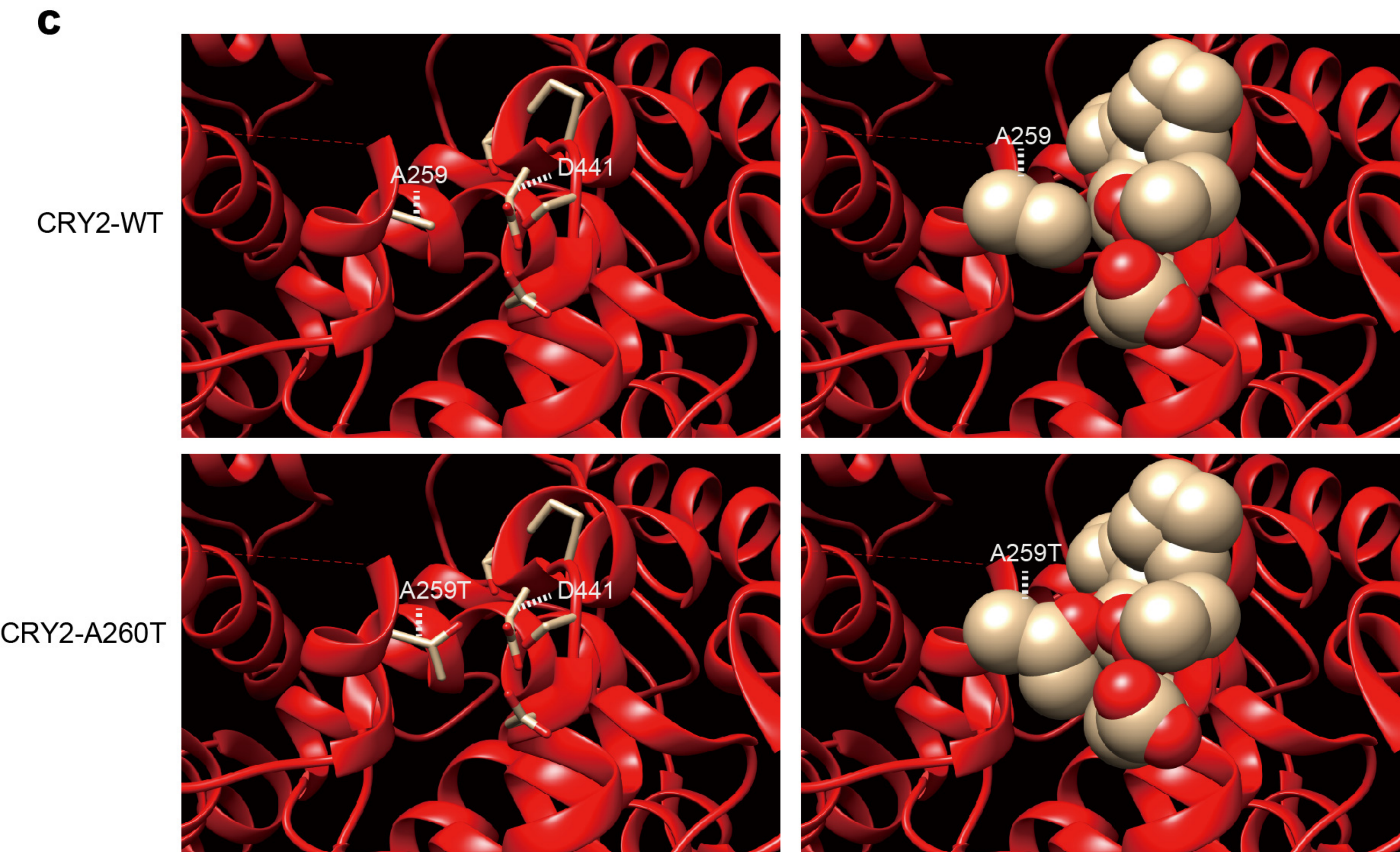
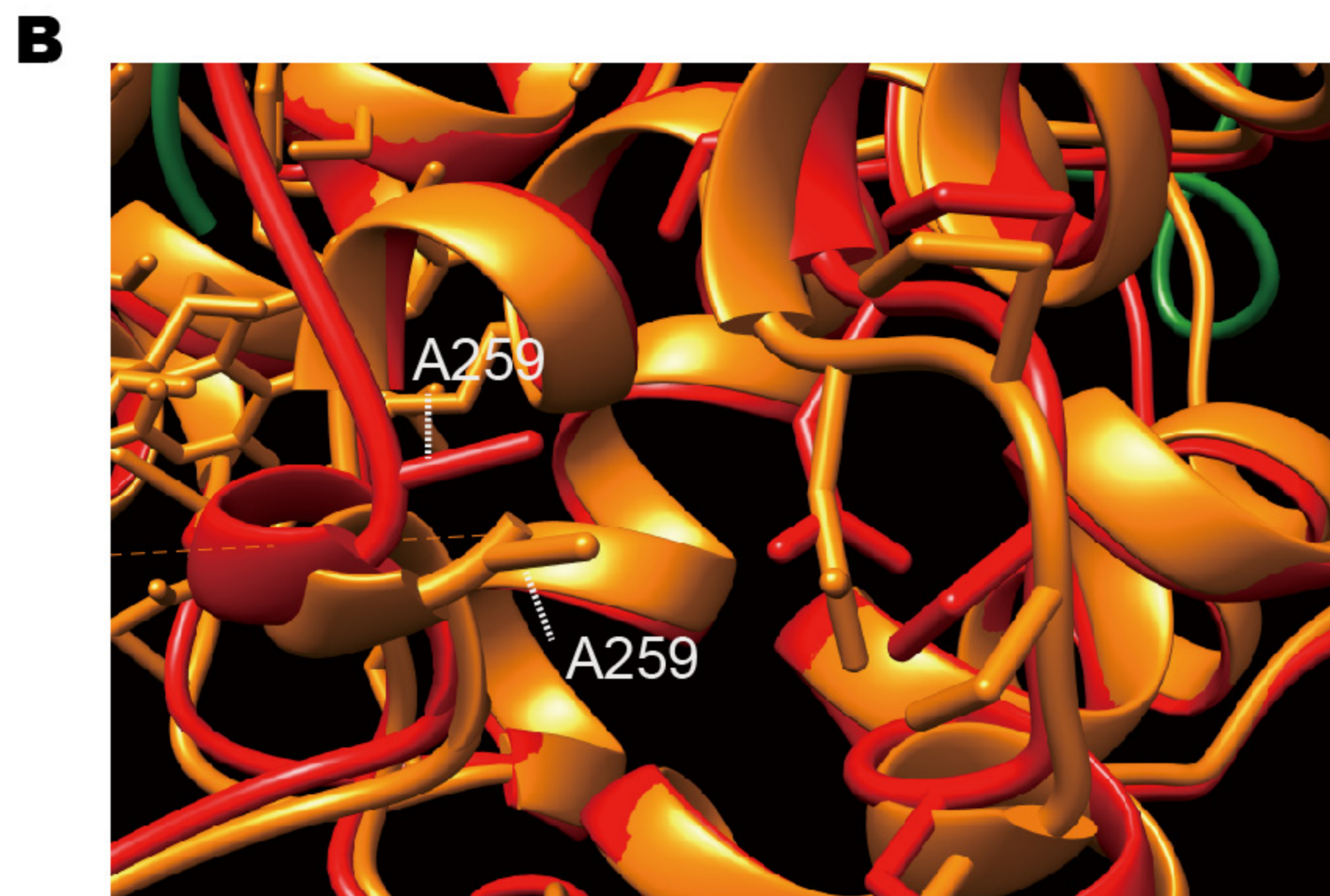
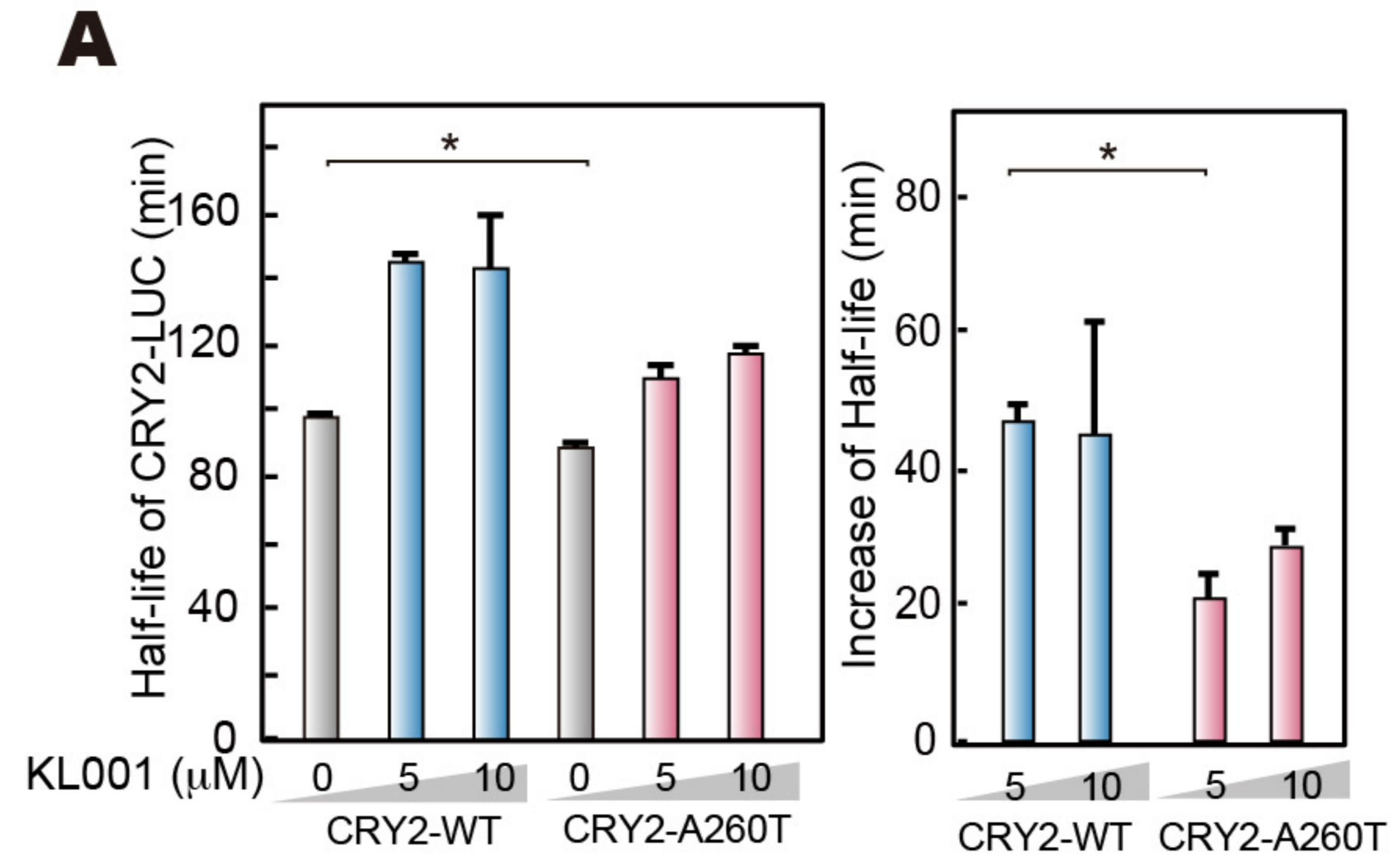


**Figure 5 - supplement 1**

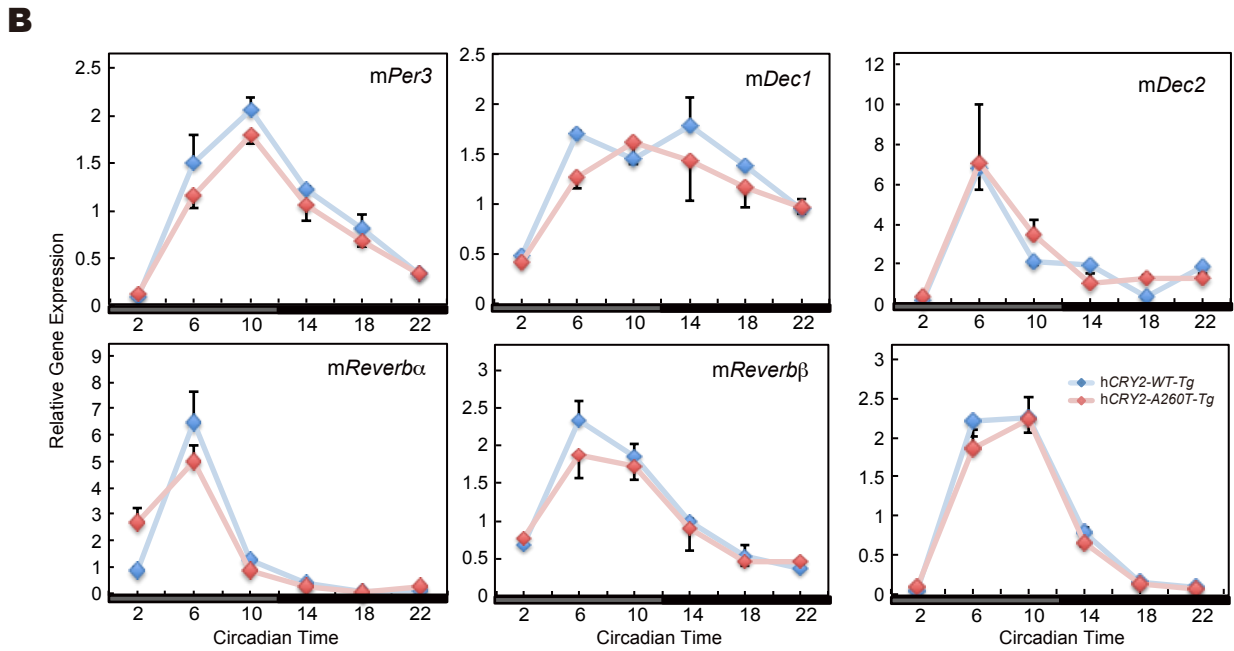
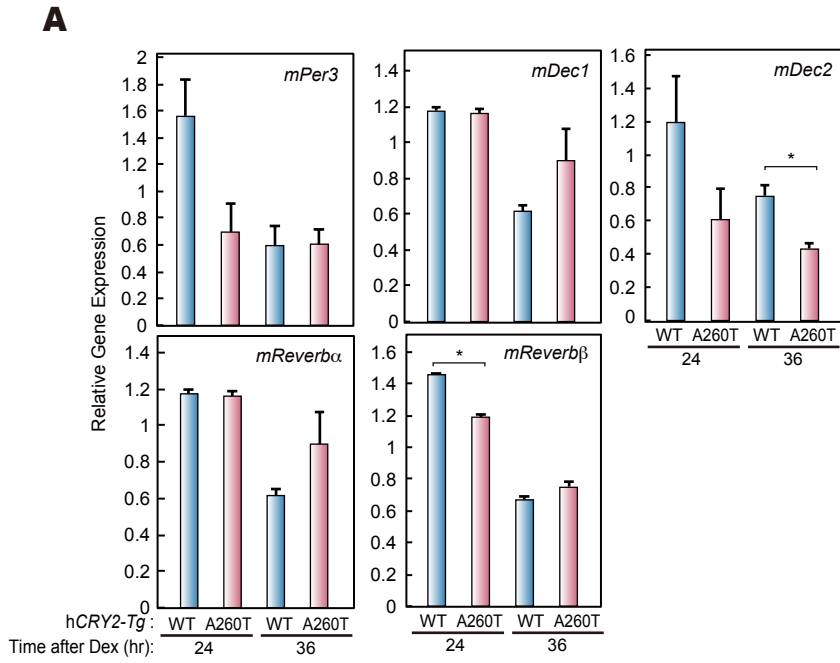


**Figure 6 - supplement 1**